Volatile Oxidation Products and Secondary Organosiloxane Aerosol from D_5 + OH at Varying OH Exposures

Hyun Gu Kang[1], Yanfang Chen[2], Yoojin Park[3], Thomas Berkemeier[1], Hwajin Kim[2,4]

[1]Multiphase Chemistry Department, Max Planck Institute for Chemistry, 55128 Mainz, Germany
[2]Department of Environmental Health Sciences, Graduate School of Public Health, Seoul National University, 08826 Seoul, South Korea
[3]Department of Environmental Science and Engineering, College of Engineering, Ewha Womans University, 03760 Seoul, South Korea
[4]Institute of Health and Environment, Graduate School of Public Health, Seoul National University, 08826 Seoul, South Korea

Correspondence to: Hwajin Kim (khj0116@snu.ac.kr) and Thomas Berkemeier (t.berkemeier@mpic.de)

Abstract. Siloxanes are composed of silicon, oxygen, and alkyl groups and are emitted from consumer chemicals. Despite being entirely anthropogenic, siloxanes are being detected in remote regions and are ubiquitous in indoor and urban environments. Decamethylcyclopentasiloxane (D_5) is one of the most common cyclic congeners, and smog chamber and oxidation flow reactor (OFR) experiments have found D_5 + OH to form secondary organosiloxane aerosol (SOSiA). However, there is uncertainty about the reaction products, and the reported SOSiA mass yields (Y_{SOSiA}) appear inconsistent. To quantify small volatile oxidation products (VOP) and to consolidate the Y_{SOSiA} in the literature, we performed experiments using a Potential Aerosol Mass OFR while varying D_5 concentration, humidity, and OH exposure (OH_{exp}). We use a proton transfer reaction time-of-flight mass spectrometer to quantify D_5, HCHO, and HCOOH, and detect other VOP, which we tentatively identify as siloxanols and siloxanyl formates. We determine molar yields of HCHO and HCOOH between 52 – 211 % and 45 – 127 %, respectively. With particle size distributions measured with a scanning mobility particle sizer, we find Y_{SOSiA} to be < 10 % at OH_{exp} < 1.3 × 10^{11} s cm^{-3} and ~20 % at OH_{exp} corresponding to that of the lifetime of D_5 at atmospheric OH concentrations. We also find that Y_{SOSiA} is dependent on both organic aerosol mass loading and OH_{exp}. We use a kinetic box model of SOSiA formation and oxidative aging to explain the Y_{SOSiA} values found in this study and the literature. The model uses a volatility basis set (VBS) of the primary oxidation products as well as an aging rate coefficient in the gas and particle phases of $k_{age,gas}$, of 1.14 × 10^{-12} cm^3 s^{-1} and $k_{age,particle}$, of 2.18 × 10^{-12} cm^3 s^{-1}. The combination of a primary VBS and OH-dependent oxidative aging predicts SOSiA formation much better than a standard-VBS parameterization that does not consider aging (RMSE = 42.6 vs. 96.5). In the model, multi-generational aging of SOSiA products occurred predominantly in the particle phase. The need for an aging-dependent parameterization to accurately model SOSiA formation shows that concepts developed for secondary organic aerosol precursors, which can form low-volatile products at low OH_{exp}, do not necessarily apply to D_5 + OH. The resulting yields of HCHO and HCOOH and the parameterization of Y_{SOSiA} may be used in larger scale models to assess the implications of siloxanes on air quality.

Keywords: D_5 siloxane, organic aerosol, proton transfer reaction mass spectrometer, oxidation flow reactor, chemical kinetics

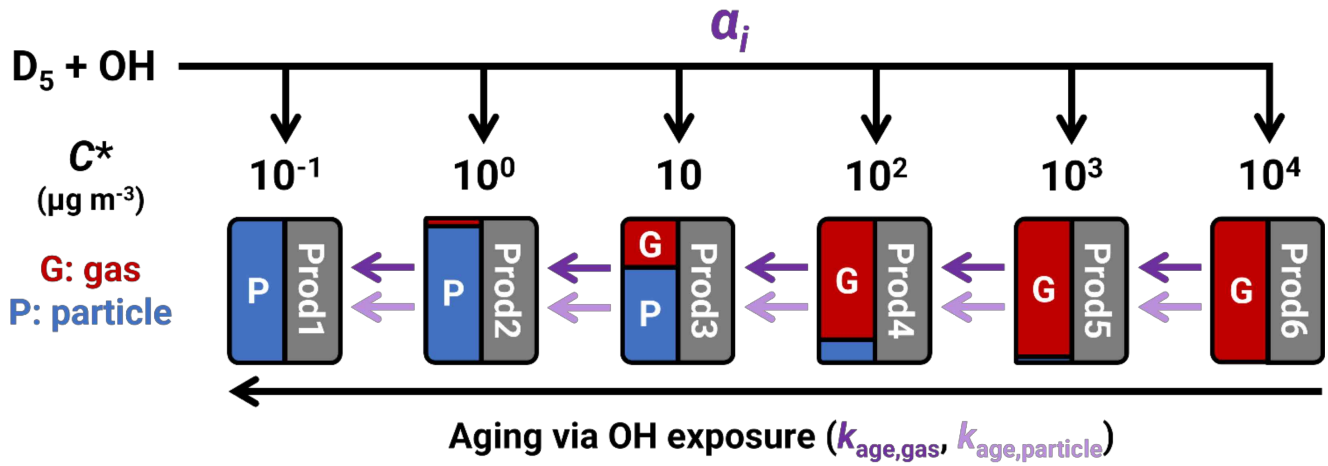

Graphical Abstract: Schematic of the kinetic box model.

1 Introduction

Organosiloxanes are molecules composed of silicon-oxygen bonds with alkyl groups on the silicons and encompass linear and cyclic species, some of which have vapor pressures on par with volatile organic compounds (VOC). Siloxanes are entirely anthropogenic pollutants (Rücker and Kümmerer, 2015) commonly used in consumer and industrial chemical products (Seltzer et al., 2021a; Gkatzelis et al., 2021) and their emissions are projected to increase in the coming decades (Tansel and Surita, 2017). Decamethylcyclopentasiloxane (D_5, $C_{10}H_{30}O_5Si_5$), where "D" refers to silicon center atoms bonded to two oxygens, is a ubiquitous cyclosiloxane in the ambient environment.

Siloxanes have been detected in the indoor environment (Tang et al., 2015; Tran and Kannan, 2015; Arata et al., 2021; Katz et al., 2021; Kaikiti et al., 2022; Wang et al., 2022), near landfills (Schweigkofler and Niessner, 1999), and sewage treatment sites (Lee et al., 2014; Horii et al., 2019). Siloxanes are also found in outdoor urban air (Xiang et al., 2021), and organosilicon compounds have been found in varying amounts in ambient particulates in China (Lu et al., 2019; Cheng et al., 2021; Meng et al., 2021; Song et al., 2022; Xu et al., 2022) and the United States (Milani et al., 2021).

Siloxanes are suspected to be environmentally persistent or emitted continuously to appear as such (Howard and Muir, 2010; Xiang et al., 2021), while other studies have found that methyl siloxanes would be removed on timescales of days to weeks (Graiver et al., 2003; Whelan and Kim, 2021). Reaction rate coefficients of D_5 with atmospheric oxidants have been reported and Atkinson (1991) found D_5 to be effectively unreactive with atmospheric concentrations of O_3 ($k_{D5+O3} < 3 \times 10^{-20}$ cm^3 s^{-1}) and NO_3 radicals ($k_{D5+NO3} < 3 \times 10^{-16}$ cm^3 s^{-1}) at ~298 K. While D_5 is reactive with OH and Cl, Alton and Browne (2020) calculated that the removal of D_5 by Cl radicals would only be a few percent of that by OH radicals at typical ambient oxidant concentrations.

Atkinson (1991), Safron et al. (2015), Xiao et al. (2015), Kim and Xu (2017), and Alton and Browne (2020) have measured k_{D5+OH} at ~298 K to be 1.55×10^{-12}, 2.6×10^{-12}, 2.46×10^{-12}, 1.46×10^{-12}, and 2.1×10^{-12} cm^3 s^{-1}, respectively. These measurements are summarized in Table S1. Xiao et al. (2015) derived k_{D5+OH} computationally as 2.90×10^{-12} cm^3 s^{-1}. In this paper, we use $k_{D5+OH} = 2.0 \times 10^{-12}$ cm^3 s^{-1}, which is a rounded average of the empirically determined rate coefficients. This k_{D5+OH} corresponds to a D_5 atmospheric lifetime of about four days via removal by OH, assuming a daily average OH concentration ($[OH]_{avg}$) of 1.5×10^6 cm^{-3}.

D_5 is expected to suppress O_3 formation in urban environments. Carter et al. (1993) performed a series of chamber experiments mimicking urban air conditions and found that D_5 siloxane would inhibit ozone formation by suppressing the OH radical. In contrast, formaldehyde (HCHO) is known to contribute to O_3 formation (Derwent et al., 1996). Fu et al. (2020 predicted the formation of HCHO as a product of D_5 + OH at low NO/HO_2 conditions using quantum chemical calculations

and kinetics modeling, but an experimental yield of HCHO from D_5 + OH has not been reported. Atkinson (1991) proposed HCHO as a product of the siloxane alkoxyl radical (RO) pathway, assuming an analogous mechanism to that of VOC. Sommerlade et al. (1993) suggested that HCHO may arise from siloxane RO decomposition and from ROOH rearrangement in the presence of acids and H_2O. Alton and Browne (2022) predicted HCHO as a product of RO_2 rearrangement in the case of D_3 siloxane. Because HCHO is a secondary product, the O_3 formation potential of D_5 may differ between source and downwind locations.

Formic acid (HCOOH) is a common acid catalyst in the atmosphere (Hazra et al., 2014) and a particle-nucleating species (Yu, 2000). Studies have identified some HCOOH sources in the atmosphere (Millet et al., 2015; Franco et al., 2021), however, HCOOH is suspected to have unidentified anthropogenic sources in the troposphere (Millet et al., 2015; Chen et al. 2021) as some urban sources remain unaccounted for (le Breton et al., 2012; Yuan et al., 2015). Chandramouli and Kamens (2001) proposed that the RO_2 initially formed from D_5 + OH makes a siloxanyl formate ($D_4T(OCHO)$), where "T" refers to a silicon center bonded to three oxygens) that reacts with H_2O to a siloxanol ($D_4T(OH)$) and HCOOH. However, we are unaware of experimental HCOOH yields reported for D_5 + OH.

Whelan et al. (2004) used known siloxane chemistry in a partitioning model to assess the atmospheric fate of siloxanes and found that silanols are the predominant oxidation products. These silanols are generally water soluble and either removed from the atmosphere via wet deposition, or undergo a pH-dependent process of hydrolysis, forming smaller and smaller silanols (Whelan et al., 2004). Eventually, the small silanols are converted to SiO_2, H_2O, and CO_2 through photolytic reactions in water or biological processes in soil (Spivack et al., 1997; Stevens, 1998; Graiver et al., 2003).

The intermediate products between D_5 and those small silanols are less studied, and the OH-oxidation rate coefficients of these intermediates have not been reported. Sommerlade et al. (1993) and Alton and Browne (2022) used mass spectrometry to study the gaseous products of D_5 oxidation in chambers, while Fu et al. (2020) used quantum chemistry modeling. These studies found that gaseous intermediates are composed of a variety of alcohols, aldehydes, esters, and hydroperoxides. Given that such volatile oxidation products (VOP) in experiments with higher OH_{exp} are likely to undergo multiple oxidation steps, there is a need to address their subsequent oxidation rate coefficients. Moreover, while the formation of HCHO and HCOOH have been predicted in mechanisms, they have not been quantified.

Secondary aerosol mass yield (Y, Eq. (1)) is defined as the ratio of produced aerosol mass (Δm(SOSiA)) to reacted precursor mass ($\Delta m(D_5)$), which we adopt here for secondary organosiloxane aerosol (SOSiA). Reports about secondary aerosol formation from D_5 siloxane seem conflicting, with some experiments reporting much higher Y_{SOSiA} than others. For instance, Wu and Johnston (2017) and Janechek et al. (2019) saw maximum Y_{SOSiA} of 23 % and 50 %, respectively, in their photo-

oxidation chamber and OFR experiments, albeit at different OH exposures (OH_{exp}). Charan et al. (2022) found a Y_{SOSiA} of 158 % with their OFR at an OH_{exp} of 3.2×10^{12} s cm^{-3}. Avery et al. (2023) reported a wide range of Y_{SOSiA} (2 – 146 %) from their OFR experiments.

$$Y_{SOSiA} = \frac{\Delta m(SOSiA)}{\Delta m(D_5)} \quad (1)$$

In contrast, Charan et al. (2022) reported almost negligible Y_{SOSiA} (< 5 %) from their chamber studies where [OH] was on the order of ~10^6 cm^{-3}, which is closer to [OH] found in ambient conditions (Peng and Jimenez, 2020). Han et al. (2022) conducted OFR experiments and found that Y_{SOSiA} would be 2 % at [OH] of 4.6×10^8 cm^{-3} or OH_{exp} of 5.5×10^{10} s cm^{-3}. The variation of Y_{SOSiA} reported in the literature suggests that oxidation conditions need to be considered to accurately parameterize Y_{SOSiA}, especially given that D_5 is being considered in air quality models as a part of volatile chemical product inventories (Pennington et al., 2021; Seltzer et al., 2021a, b).

In this study, we aim to assess the OH-oxidation of D_5 by determining rate coefficients of secondary reactions of VOP with OH (i.e., chemical aging) and providing a first quantification of HCHO and HCOOH yields. We also measure Y_{SOSiA} under diverse OH_{exp} and $[D_5]_0$. Lastly, we develop parameterizations of SOSiA yield using a kinetic model with chemical aging reaction scheme to reconcile the reported Y_{SOSiA} from D_5 + OH in the literature and for use in air quality models.

2 Method and Materials

2.1 Experiments

The Aerodyne Research (Billerica, MA, USA) potential aerosol mass OFR (PAM-OFR) (Kang et al., 2007) has a volume of 13.3 L and is made of chromated aluminum (Xu and Collins, 2021). We operated the PAM-OFR in "OFR185" mode (Peng and Jimenez, 2020), where 185 nm lamps that also emit 254 nm light (GPH436T5VH, LightSources, Orange, CT, USA) generate OH and O_3 with injected H_2O vapor from a Nafion humidifier (FC-100-80-6MKK, Perma Pure, Lakewood, NJ, USA). There were two of these 185 nm lamps placed across from each other in clear fused quartz sleeves. The 185 nm lamps were wrapped with covers at even intervals to reduce the UV intensity so that 90 % of the lamp surface was covered. We operated the PAM-OFR at residence times (τ_{res}) of 120 and 180 s with flow rates of 6.65 and 4.43 L min^{-1}, respectively. Additional details about the experiment setup are summarized in Fig. S1 and Sect. S1.

We use the D_5 siloxane trace measured from the proton transfer reaction mass spectrometer (PTR-MS) to calculate OH_{exp} with Eq. (2), where $k_{D5+OH} = 2.0 \times 10^{-12}$ cm^3 s^{-1}. $[D_5]_0$ and $[D_5]_{final}$ are the D_5 concentrations before and after the exposure to OH.

$$OH_{exp} = -\frac{1}{k_{D5+OH}} \times \ln\left(\frac{[D_5]_{final}}{[D_5]_0}\right) \quad (2)$$

Prior to experiments, we checked the background particle and D_5 concentrations with the scanning mobility particle sizer (SMPS) and PTR-MS. In all experiments, the background particle number concentrations were < 10 cm^{-3}, and the background $[D_5]$ were below the limit of detection (3σ = 80 ppt). Then, we injected D_5 with a syringe pump while monitoring the PTR-MS, with major ions at *m/z* 371 and *m/z* 355. We performed the experiments with target $[D_5]_0$ of 50, 100 or 200 ppb. With these target $[D_5]_0$, we get external OH reactivities (OHR_{ext}) of 2.5 – 9.8 s^{-1} at 298.15 K and 1 atm, where OHR_{ext} is the reactivity caused by the injection of D_5 into the PAM-OFR (Peng and Jimenez, 2020). With these OHR_{ext}, we reduce the risk of OH suppression and VOC photolysis (Peng and Jimenez, 2020).

When the D_5 trace stabilized near the target $[D_5]_0$, we began the experiment by turning on the UV lamps in the PAM-OFR to either 2.4 or 8.0 V. We waited 30 minutes for the UV lamps to stabilize and for the PAM-OFR walls to equilibrate with gaseous species. The Y_{SOSiA} (Eq. (1)) were calculated using the average SOSiA mass concentration from four SMPS cycles following those 30 minutes. We obtained $\Delta m(D_5)$ as the difference between $[D_5]_0$ and $[D_5]_{final}$. At the end of an experiment, we turned off the UV lamps to check the D_5 trace return.

To clean the PAM-OFR between experiments, we stopped the syringe pump and removed the syringe from the glass bulb while keeping the humid air flow through into the PAM-OFR. We turned on the PAM-OFR UV lamps and connected the outlet directly to the exhaust, until D_5 and particle number concentrations we below the limit of detection. We used Igor Pro 9 (Wavemetrics, Portland, OR, USA) for data post-processing and visualization.

2.2 Instrumentation

2.2.1 PTR-MS

To measure D_5 and VOP, we used a PTR-MS (PTR-TOF 1000, Ionicon Analytik, Innsbruck, Austria) equipped with the extended volatility range (EVR) option (Piel et al., 2021), where the wetted inlet components and the drift tube are passivated with a silicon coating. The PTR-MS also had ion transfer lens between the drift tube and time-of-flight mass spectrometer (Jordan et al., 2009). An internal permeation source (PerMaSCal) emitted a steady stream of 1,3-diiodobenzene into the mass spectrometer for mass calibration scale adjustments. Additional PTR-MS details are in Sect. S1.

To reduce H_2O clusters at high humidities, we operated the PTR-MS at 137 Td (U_{drift} = 600 V, Td = Townsend, 1 Td = 10^{-17} V cm^2) for quantification. The drift tube pressure and temperatures were set to 2.30 mbar and 80 °C. For the reagent ion

source, we set the U_s, U_{so}, and the H_2O flow rate to 150 V, 80 V, and 6.00 sccm respectively. The ion source hollow cathode discharge current was set to 5.0 mA. The PTR-MS drift tube was 9.6 cm long, and at 137 Td, the $[H_2O]H^+$ reaction time (Δt) was 94 μs (de Gouw et al., 2003). We calculate the primary reagent ion signal, $[H_2O]H^+$, by multiplying the signal of its isotope, $[H_2{}^{18}O]H^+$, by 500.

We use the PTR-MS data for the quantification of D_5 (*m/z* 371), HCHO (*m/z* 31), and HCOOH (*m/z* 47), where the primary reagent ion counts were normalized to 10^6 counts per second (ncps). For D_5, we used a calibration gas cylinder (Apel-Riemer Environmental, Miami, FL, USA) containing D_5 to calibrate the PTR-MS. We also calculate the normalized measurement sensitivity (ncps ppb^{-1}) of D_5, HCHO, and HCOOH using Eq. (3) adapted from de Gouw and Warneke (2007). $I_{(VOC)H^+}$ and $I_{(H2O)H^+}$ are the ion counts of the protonated VOC and the reagent ion respectively. Additional details on the mass spectra interpretation and quantification are in Sect. S1.5 and S3.

$$\text{Sensitivity} = \frac{\frac{I_{(VOC)H^+}}{I_{(H_2O)H^+}} \times 10^6}{[VOC]} \quad (3)$$

We tested the instrument sensitivity response with humidity by keeping the species concentrations constant while changing the sample air humidity. The sensitivity of D_5 at *m/z* 371 was not heavily affected by humidity at 137 Td, and we did not correct for humidity in the D_5 quantification (Fig. S5). On the other hand, HCHO and HCOOH sensitivities varied with humidity, and we corrected their sensitivities as detailed in Sect. S3. Prior to experiments, we tuned the micro channel plate (MCP) to prevent signal bias against higher mass ions (Müller et al., 2014). We adjusted the MCP voltage in steps to increase the signal strength at *m/z* 331, a diiodobenzene ion, until the relative signal increase was < 20 %.

2.2.2 Scanning Mobility Particle Sizer

An SMPS (Model 3938, TSI, Shoreview, MN, USA) equipped with an impactor (0.0508 cm) measured the particle mobility diameter size distribution between diameters of 14.3 to 723.4 nm. The SMPS consisted of a Model 3082 Electrostatic Classifier, a Model 3081A Differential Mobility Analyzer (DMA), a Model 3088 Soft X-ray Neutralizer, and a Model 3756 Ultrafine Condensation Particle Counter. We set the SMPS sheath flow at 3.0 L min^{-1} and the aerosol flow rate at 0.3 L min^{-1}, and the DMA voltage ranged from 10.6 to 9921.4 V. The SMPS scanned for 150 s, followed by a 5 s retrace and 10 s purge while recording on a 3 min cycle. We referred to the manufacturer's recommendations when deciding the above SMPS settings (TSI Inc., 2012), and a sample particle size distribution from experiment 12 (Table 1) is shown in Fig. S4.

For the Y_{SOSiA} calculations, we convert the SMPS integrated particle volumes into mass using a SOSiA mass density (ρ_{SOSiA}) of 1.07 g cm^{-3} for all experiments. We obtained this ρ_{SOSiA} from PAM-OFR experiments separate from the ones described

here, where we weighed the masses of SOSiA collected on filters and obtained particle volumes with the SMPS. Additional details on ρ_{SOSiA} are available in Sect. S2.

2.3 Volatility Distribution Parameterization

Janechek et al. (2019) and Charan et al. (2022) fitted their Y_{SOSiA} data to the Odum two-product model (Odum et al., 1996) and we follow the same methodology for comparison with the literature (Sect. S4). Similarly, we fit the standard volatility basis set (VBS) parameters α (Donahue et al., 2006) in Eq. (4) to the measured Δm(SOSiA) using the measured Δm(D_5), where α_i is the product mass yield for volatility bin i.

$$\Delta m(SOSiA) = \Delta m(D_5) \times \sum_{i=1}^{n} \frac{\alpha_i}{1 + \frac{C_i^*}{C_{OA}}} \quad (4)$$

In the experiments, the organosiloxane aerosol mass loading (C_{OA}) was equivalent to the SOSiA mass concentrations. As the produced aerosol mass in the experiments ranged from 3.7 to 965.7 μg m^{-3}, we use six logarithmically spaced effective saturation mass concentration (C^*) bins ranging from 0.1 to 10 000 μg m^{-3} at 298.15 K to cover the low and high-volatility products. For reference, D_5 liquid has a vapor pressure of 20.4 Pa at 298.15 K or $C^* = 3.05 \times 10^6$ μg m^{-3} (Lei et al., 2010). Since the experiments had slight variations in temperature, we correct for temperature impacts on C^* between experiments using the Clausius-Clapeyron equation and an enthalpy of vaporization of 60 kJ mol^{-1}, which is that of D_5 siloxane (Lei et al. 2010).

As the experiments were performed for a range of OH_{exp}, the products between experiments may have varied due to multigenerational aging (Zhao et al., 2015). To account for aging and parameterize Y_{SOSiA} as a function of OH_{exp}, we also analyse the yield data using a kinetic box model with four chemical reactions (Eq. (R1) – (R3)) written in MATLAB (MathWorks, Natick, MA, USA).

$$D_5 + OH \rightarrow \sum \alpha_i \times \text{prod}(i) \quad (k_{D5+OH} = 2.0\times10^{-12}\ \text{cm}^3\ \text{s}^{-1}) \quad \text{(R1)}$$

$$(1\text{-}f_i) \times \text{prod}(i) + OH \rightarrow (1\text{-}f_i) \times \text{prod}(i\text{-}1) \quad (k_{age,gas},\ i = 2, \ldots, 6) \quad \text{(R2)}$$

$$f_i \times \text{prod}(i) + OH \rightarrow f_i \times \text{prod}(i\text{-}1) \quad (k_{age,particle},\ i = 2, \ldots, 6) \quad \text{(R3)}$$

Eq. (R1) describes the initial oxidation of D_5 and immediate formation of products of varying volatility. Here, prod(i) refers to the sum of products (gas + particle) in volatility bin i, which are formed with a molar branching ratio α_i. We assume that prod(i) have the same molecular weights (g mol^{-1}) as D_5, and so the α_i are equivalent to the product mass yields at $OH_{exp} \rightarrow 0$

In the model, a fraction f_i of each oxidation product partitions instantaneously from the gas phase to the particle phase according to absorptive partitioning theory (Donahue et al., 2006) (Eq. (5)).

$$f_i = \left(\frac{1}{1 + \frac{C_i^*}{C_{OA}}} \right) \quad (5)$$

Eqs. (R2) and (R3) describe how OH_{exp} causes volatility to decrease (Robinson et al., 2007). This decrease in volatility via "bin-hopping" (Sommers et al., 2022) occurs at a rate proportional to the chemical aging rate coefficients for gas and particle-phase species ($k_{age,gas}$ and $k_{age,particle}$, $cm^3\ s^{-1}$). Here, we assume that products in the lowest-volatility bin (i = 1) cannot be removed from that bin and that the highest-volatility bin (i = 6) does not receive product with aging. The [OH] are set by dividing the experimental OH_{exp} from Eq. (2) by the PAM-OFR residence times.

We use $k_{age,gas}$ and $k_{age,particle}$ as aggregate chemical aging rate coefficients, not specific to any species or volatility bin. Studies on chamber experiments (Robinson et al., 2007) and ambient measurements (Sommers et al., 2022) applied chemical aging only to the gas phase as heterogeneous aging is relatively slower. However, studies have found that the high oxidant concentrations in OFRs would appreciably oxidize OA within experiment timescales (Kessler et al., 2012; Kroll et al., 2015). To accommodate OH uptake to the bulk phase, we include particle-phase aging that also decreases the volatility of particle-phase products. The timescales and atmospheric relevance of heterogeneous oxidation in OFRs are areas of ongoing research (Zhao et al., 2019; Peng and Jimenez, 2020), but for now we opt to fit chemical aging rate coefficients for each phase.

We fit $k_{age,gas}$, $k_{age,particle}$, and α_i in the aging-VBS model to the experimental SOSiA mass using the Monte Carlo genetic algorithm (MCGA) (Berkemeier et al., 2017). We obtain a best model fit and a fit ensemble consisting of 548 parameter sets for which the model's root mean square error (RMSE) is below a threshold of 50. We find this ensemble to estimate the parametric uncertainty associated with the model fit (Berkemeier et al., 2021).

We use the OFR chemistry template with KinSim (Peng and Jimenez, 2020) to estimate the RO_2 fates and expect the fates to have been uniform across the experiments (Sect. S5). Although there are uncertainties in the RO_2 reaction rate coefficients for siloxanes, we expect that the variation in Y_{SOSiA} is not driven by RO_2 fate in these experiments. We also report the condensational sink and condensation lifetimes (Palm et al., 2016) calculated using the particle size distributions in Sect. S1.3.

3 Results and Discussion

3.1 Volatile Organic Products (VOP)

3.1.1 Siloxanol and Formate Ester Trends

In Fig. 1, the PTR-MS signals before and after D_5 is oxidized are displayed relative to the protonated D_5 ion at *m/z* 371 on the y-axis. We perform this scaling because the isotopologues of the product fragment ions overlap with the isotopologues of D_5. Thus, changes in signal intensity are caused by both product formation and D_5 oxidation. We choose to normalize the spectra at *m/z* 371 because we assume that no product ion peaks overlap with the $[D_5]H^+$ signal at *m/z* 371. While this scaling makes the product peaks appear larger, the changes in the mass spectrum are also qualitatively highlighted. For example, D_5 loses a methyl group during the PTR, which forms a large signal at *m/z* 355. The isotopologues of the $-CH_4$ fragment of $[D_5]H^+$ overlap with fragments of VOP. By scaling the mass spectrum with the ratio of $[D_5]H^+$ signal before and after oxidation, the signal of the VOP is separated from that of remaining D_5.

Using the mass spectra and species reported by Alton and Browne (2022), we attribute the indicated ions in Fig. 1 to siloxanol ($D_4T(OH)$), siloxanediol ($D_3T_2(OH)_2$), siloxanyl formate ($D_4T(OCHO)$), and siloxanolyl formate ($D_3T_2(OH)(OCHO)$). Here, "D" and "T" refers to silicon centers bonded to two and three oxygen atoms respectively. The multifunctional VOP are reported to arise from multiple steps of oxidation (Alton and Browne, 2022). The red and pink shaded areas in the inset of Fig. 1 refer to the enhancement in signal over that of the $-CH_4$ fragment of $[D_5]H^+$, which we attribute to the $-H_2O$ fragments of $[D_4T(OH)]H^+$ and $[D_3T_2(OH)_2]H^+$, respectively. We use the masses of the $-H_2O$ fragments of the protonated siloxanols as large alcohols dissociate during the PTR (Brown et al., 2010). We also attribute the ions in the blue and yellow-dotted boxes to the $-H_2O$ fragments of $[D_3T_2(OH)(OCHO)]H^+$ and $[D_4T(OCHO)]H^+$.

As we did not have calibration standards to quantify these VOP, we calculate the molar yields of the VOP relative to that of protonated D_5 siloxane at *m/z* 371 to study the trends of siloxane VOP (Fig. 2). For each VOP, we choose a characteristic peak in the mass spectrum and calculate the change in signal due to VOP formation (Sect. S1.5). Then, we calculate the ratios of the changes in the VOP and D_5 signals to get the relative molar yields ($Y_{\mathrm{rel,VOP}i}$). In the right-side panels for each VOP in Fig. 2, the $Y_{\mathrm{rel,VOP}i}$ decreases with increasing OH_{exp} (x-axes). This decrease in VOP signal is consistent with these gaseous products undergoing further oxidation or increased gas-particle partitioning due to higher C_{OA} at higher OH_{exp}. We use the colors to highlight the functional groups on the D_5 backbone.

In the left-side panels for each VOP in Fig. 2, the relative signals of the VOP (y-axes) decrease with increasing OH_{exp} (color scale). Then, assuming that [OH] is constant throughout the PAM-OFR, that D_5 + OH is the rate-limiting step in VOP formation, and that removal via gas-particle partitioning is negligible (Alton and Browne, 2022), we can consider a simplified D_5 + OH chemical mechanism, Eqs. (R4) and (R5).

$$D_5 + OH \rightarrow \sum \gamma_i VOP_i \qquad (k_{D5+OH} = 2.0 \times 10^{-12}\ cm^3\ s^{-1}) \qquad (R4)$$

$$VOP_i + OH \rightarrow \qquad (k_{VOPi+OH}) \qquad (R5)$$

In Eq. (R4), γ_i is the relative molar yield of a given VOP_i found by extrapolating $Y_{rel,VOPi}$ (y-axes in Fig. 2) to $OH_{exp} \rightarrow 0$. With ordinary differential equations from these reactions (Eqs. (7) and (8)) and experimental inputs, we fit γ_i and the VOP_i + OH rate coefficient ($k_{VOPi+OH}$, $cm^3\ s^{-1}$). The fits are shown as black lines in the right-side panels of each VOP in Fig. 2.

$$\frac{d[D_5]}{dt} = -k_{D5+OH}[D_5][OH] \qquad (7)$$

$$\frac{d[VOP_i]}{dt} = \gamma_i k_{D5+OH}[D_5][OH] - k_{VOPi+OH}[VOP_i][OH] \qquad (8)$$

The fitted $k_{VOPi+OH}$ for each VOP are on the order of ~10^{-12} $cm^3\ s^{-1}$ (Table S7), but faster than k_{D5+OH}, which suggests that these VOP have atmospheric lifetimes shorter than that of D_5. Alton and Browne (2022) have estimated these VOP to be volatile with quantitative structure activity relationship models. However, there are uncertainties in those models, and the VOP may have lower saturation mass concentrations than expected. Moreover, the chemical mechanism might be more complex than the one outlined with the simple reactions (R4) and (R5). Consequently, we present these $k_{VOPi+OH}$ as estimates for secondary chemistry in this simplified reaction scheme, and future work using quantitative measurements should improve the calculated lifetimes of these intermediate D_5 + OH products in the atmosphere.

3.1.2 Formaldehyde (HCHO) Yields

As shown in Table S8 and Fig. 3, the experimental molar yields of HCHO (Y_{HCHO}, $\Delta HCHO/\Delta D_5$ in ppb/ppb) exceed 100 % at low OH_{exp} and decrease with higher OH_{exp}. We attribute the decreasing Y_{HCHO} with increasing OH_{exp} to HCHO removal by OH in the PAM-OFR. HCHO has a lifetime of 0.91 days at $[OH]_{avg} = 1.5 \times 10^6$ cm^{-3} (Atkinson et al., 2006) or 78 s at [OH] = 1.5×10^9 cm^{-3}. In such high [OH] conditions, some HCHO is oxidized while being produced, which is consistent with the decreasing Y_{HCHO} with increasing OH_{exp} (Fig. 3a). However, HCHO formation likely occurs over multiple oxidation steps (Fu et al., 2020), and how VOP + OH branches to produce HCHO and the rate coefficients for those reactions are not experimentally constrained.

Consequently, we implement a simplified mechanism (Eqs. (R6) – (R8)), where D_5 + OH produces a representative VOP (VOP_{rep}) and yields HCHO at each oxidation step. The subsequent VOP_{rep} + OH reactions share the same rate coefficient as D_5 + OH and produce HCHO with the same yield (γ_{HCHO}). This γ_{HCHO} is the cumulative molar yield of HCHO, or the molar

yield of HCHO as $OH_{exp} \rightarrow 0$. This γ_{HCHO} is also used to correlate satellite column retrievals of HCHO with VOC emissions (Millet et al., 2006), where an empirical value can be used to constrain uncertainty.

$$D_5 + OH \rightarrow VOP_{rep} + \gamma_{HCHO}HCHO \quad (k_{D5+OH} = 2.0 \times 10^{-12}\ cm^3\ s^{-1}) \quad (R6)$$

$$VOP_{rep} + OH \rightarrow VOP_{rep} + \gamma_{HCHO}HCHO \quad (k_{D5+OH}) \quad (R7)$$

$$HCHO + OH \rightarrow \quad (k_{HCHO+OH} = 8.5 \times 10^{-12}\ cm^3\ s^{-1}) \quad (R8)$$

We fit γ_{HCHO} to be 223 % (black line in Fig. 3a), assuming a constant [OH] in the PAM-OFR and that HCHO removal via partitioning or reactive uptake is negligible. This γ_{HCHO} is consistent with the modeled yields of those for VOC used by Millet et al. (2006), who used γ_{HCHO} from chemical models ranging from 60 – 230 % for a variety of VOC. Thus, D_5 has a comparable γ_{HCHO} to that of isoprene or aromatic VOC. An improved mechanism and additional rate coefficients are needed to accurately model HCHO formation.

Fu et al. (2020) proposed a mechanism for D_3 siloxane, where high Y_{HCHO} is produced under low NO/HO_2 conditions. In that mechanism, RO_2 rearrangement and RO H-shift is fast, and HCHO is produced at each rearrangement step. The γ_{HCHO} exceeding 100 % in these D_5 experiments is consistent with HCHO production over multiple rapid oxidation steps. The results we report suggests that a similar HCHO production mechanism exists for D_5.

Mao et al. (2009) found that models under-predicted tropospheric HCHO during their aircraft campaign studying Asian pollution outflows into the Pacific Ocean. This discrepancy between the measurements and calculations was pronounced near the surface and up to 2 km. They proposed that there is some missing OH reactivity, and that the unaccounted species would be reactive with OH and yield HCHO when oxidized. Based on the D_5 experiments present here, the inclusion of siloxane species may reduce the HCHO formation gap; Coggon et al. (2021) already noted that including volatile chemical products in their model would increase HCHO production.

The large formation of HCHO may entail that D_5 siloxane could contribute to O_3 formation, albeit indirectly. We were unable to observe O_3 enhancement due to the high concentrations of O_3 produced from the PAM-OFR internal chemistry itself and the lack of NO_x. Given that k_{D5+OH} is relatively slow compared to that of other common anthropogenic VOC, we suspect that the oxidation of D_5 will occur downwind of urban sources in low-NO_x conditions or in cases of air stagnation. Whether D_5 has a net positive or negative effect on O_3 formation in these VOC/NO_x scenarios needs to be assessed with models. To get a rough estimate of O_3 production, we consider a case where 20 ppt of D_5 react with OH to form 40 ppt of HCHO, which also fully react. This D_5 concentration is within the range reported by Coggon et al. (2018) in ambient urban air. The molar maximum incremental reactivity of HCHO under high-NO_x conditions is ~20 % (Carter et al., 1995), which makes HCHO a

prominent precursor for tropospheric O_3. By multiplying the MIR with the HCHO reacted with OH, we can estimate an O_3 formation potential of 8 ppt from D_5 in urban air.

3.1.3 Formic Acid (HCOOH) Yields

We find molar yields of HCOOH (Y_{HCOOH}, $\Delta HCOOH/\Delta D_5$ ppb/ppb) between 45 – 127 %, as shown in Fig. 3b, although a trend with OH_{exp} is not obvious (Fig. 3b).We assume HCOOH loss via OH oxidation to be minor given the rate coefficient of $k_{HCOOH+OH} = 4.5 \times 10^{-13}$ cm^3 s^{-1} at 298.15 K (Atkinson et al., 2006), which corresponds to 17 days of OH_{exp} at $[OH]_{avg} = 1.5 \times 10^6$ cm^{-3} or an OH-oxidation lifetime of 440 s in our highest OH_{exp} experiment. In addition to D_4T(OCHO) hydrolysis, HCOOH may have been produced by heterogeneous reactions of HCHO at the surface of the SOSiA or the OFR walls in these humid experiments. In the atmosphere, HCOOH is presumed to form heterogeneously from HCHO and methanediol ($HOCH_2OH$) in the presence of wet particles (Franco et al., 2021).

The Y_{HCOOH} from D_5 + OH we report are higher than the values from isoprene + OH (Link et al., 2020) or monoterpene + OH reported by Friedman and Farmer (2018), who quantified the Y_{HCOOH} of seven monoterpenes at varying OH_{exp} without NO_x. The range of Y_{HCOOH} from these references is shown as shaded areas in Fig. 3b. The Y_{HCOOH} from D_5 is on par with the humid isoprene ozonolysis cases reported by Link et al. (2020). Friedman and Farmer (2018) also used a PAM-OFR, but with 254 nm UV lamps in dry conditions (~1 % RH), and Link et al. (2020) used a reaction chamber, which limits a direct comparison with our results. Nevertheless, Friedman and Farmer (2018) found Y_{HCOOH} of 0.64 – 8.5 % at $OH_{exp} = 2.0 \times 10^{11}$ s cm^{-3}. Aside from the different precursor VOC and mechanism, Friedman and Farmer (2018) may have encountered less heterogenous production of HCOOH due to the dry OFR conditions. While D_5 + OH may produce more HCOOH than isoprene + OH, the global emissions of D_5 (McLachlan et al., 2010) are about four orders of magnitude smaller than those of isoprene (Guenther et al., 2012). Nevertheless, the product class of siloxanes may constitute a minor atmospheric HCOOH source in urban locations, especially if emissions were to increase.

3.2 SOSiA Mass Yields

3.2.1 Volatility Basis Set Parameterization

The Odum two-product model does not accurately capture the Y_{SOSiA} in the literature in the high C_{OA} range (Sect. S4), so we apply a VBS model. Fig. 4a shows the fitted aerosol mass yield curve (blue line) using a standard-VBS model (Eq. (4)), but the experimental Y_{SOSiA} (y-axis) appears to depend on both C_{OA} (x-axis) and OH_{exp} (color scale). To address whether accounting for the varying OH_{exp} in these experiments would improve the VBS model outputs, we fit the produced SOSiA mass using a standard-VBS model (Eq. (4)) and a kinetic model with VBS and chemical aging rate coefficients ("aging-VBS model", Eqs. (R1) – (R3)) based on OH_{exp} and $[D5]_0$ (Table 1).

We fit $k_{age,gas}$ and $k_{age,particle}$ in the aging-VBS model to be 1.14×10^{-12} cm^3 s^{-1} and 2.18×10^{-12} cm^3 s^{-1} respectively. The fitted aging-VBS model parameters are summarized in Table S11. Fig. 4a also shows the aerosol mass yield curves calculated with the aging-VBS model over varying OH_{exp}. Since the aging-VBS model is kinetic, the Y_{SOSiA} are dependent on both $[D_5]_0$ and OH_{exp}, and we calculate three yield curves using the approximate experimental $[D_5]_0$. The yield curves generated with the aging-VBS model are more consistent with the experiments and show how Y_{SOSiA}, $[D_5]_0$, and OH_{exp} are intertwined in the proposed aging mechanism.

Secondary organic aerosol (SOA) mass yield often exhibits a maximum as a function of OH_{exp}, after which the yield decreases due to fragmentation becoming dominant at high OH_{exp} (Isaacman-VanWertz et al., 2018). We do not find such a maximum in the range of OH_{exp} studied, which suggests that an even higher Y_{SOSiA} could have been found at higher OH_{exp}. Moreover, SOSiA is reported to be non-hygroscopic compared to SOA (Janechek et al., 2019), and we do not see an obvious relationship between the experiment humidity conditions and aerosol formation.

In both the standard and aging-VBS model fits (blue and red, respectively in Fig. 4b), ~95 % of the D_5 + OH product mass is in the gas phase at a C_{OA} of 10 μg m^{-3}. The high fraction of gaseous products is consistent with low Y_{SOSiA} in the lower OH_{exp} experiments, whereas additional oxidation in the higher OH_{exp} experiments leads to a shift towards products that partition into the particle phase, thus increasing Y_{SOSiA}. The optimized α_i for the aging-VBS model are shown as markers in Fig. 4b. The error bars indicate the minimum and maximum values of the fitted α_i in the ensemble parameter sets, which are further expanded in Fig. S12a. The fit ensemble suggest that products from D_5 + OH must be largely volatile ($C^* \geq 10^3$ μg m^{-3}) in order to reproduce the experimental SOSiA yields.

Figs. 4c and 4d show comparisons of the standard and aging-VBS models with experimental SOSiA mass concentrations and Y_{SOSiA}. The error bars indicate the range of model outcomes within the fit ensemble. We see an improvement in the RMSE and R^2 with the aging-VBS over the standard-VBS model, suggesting that incorporating OH_{exp} into the yield parameterization improves model performance. Fig. 5 compares the standard-VBS model with the aging VBS for a range of OH_{exp}, showing that product volatility gradually decreases with increasing OH_{exp} in the aging-VBS model. The high volatility of the initial products is consistent with the lack of the rapid formation of low-volatile species, such as highly-oxygenated molecules known to form SOA (Isaacman-VanWertz et al., 2018).

We find that the model is very sensitive to $k_{age,particle}$, as a higher $k_{age,particle}$ will result in higher model SOSiA formation (Fig. S11a), but not sensitive to $k_{age,gas}$. In addition, $k_{age,particle}$ is tightly constraint in the ensemble of model fits around a value of 2×10^{-12} cm^3 s^{-1} (Fig. S12b). When fitting the model with deactivated particle-phase aging ($k_{age,particle} = 0$), model-experiment RMSE is significantly increased and the fitted $k_{age,gas}$ becomes unphysically large. The numerical value of the fitted $k_{age,particle}$,

on the other hand, is physically reasonable as it corresponds to an effective uptake coefficient of OH molecules colliding with the particle surface of less than one (Sect. S1.6). We hence postulate that multi-generational aging of SOSiA occurs predominantly in the particle phase.

3.2.2 Consolidating Literature Y_{SOSiA}

To address the variation in the literature Y_{SOSiA} and to generate parameters for air quality models, we fit the parameters in the aging-VBS model with all available data in the literature and those from our experiments. Given that the literature used differing ρ_{SOSiA} to calculate Y_{SOSiA} from SMPS data, we adjust the Y_{SOSiA} and C_{OA} reported in the literature to that of the ρ_{SOSiA} used here (ρ_{SOSiA} = 1.07 g cm^{-3}). Similarly, we re-calculate the OH_{exp} in the literature using Eq. (2) and the $[D_5]_0$ and $[D_5]_{final}$ values.

Fig. 6 shows experimental values (markers) and model outputs (contours) of Y_{SOSiA} (panels a1 and a2) and SOSiA mass concentrations (panels b1 and b2) as a function of $[D_5]_0$ and OH_{exp}. Figs. 6a1 and 6b1 are generated using the aging-VBS model fit using only data from experiments presented in this study, while Figs. 6a2 and 6b2 show a fit including data from the literature. The aging-VBS model captures the increasing Y_{SOSiA} with increasing $[D_5]_0$ and OH_{exp}. At a given $[D_5]_0$, Y_{SOSiA} and the SOSiA mass concentrations increase with higher OH_{exp}. Fig. 6a2 shows that the relatively high Y_{SOSiA} (> 50 %) is feasible at $OH_{exp} > 10^{12}$ s cm^3. Moreover, the aging-VBS model predicts that Y_{SOSiA} is almost negligible (< 5 %) under atmospheric concentrations of D_5 and OH_{exp}.

Fig. S8 shows that the aging-VBS model used here leads to a much higher correlation between modelled and experimental values for SOSiA mass concentration compared to the same analysis with a standard-VBS model (RMSE = 105 vs. 259). The better correlation suggests that the volatility distribution evolves with OH_{exp} and that chemical aging should be considered when evaluating the volatility distribution of SOSiA from D_5 + OH.

We note that bulk-phase chemistry is more complex than logarithmic shifts in volatility with OH_{exp} and not fully captured in the proposed aging-VBS parameterization. For example, Wu and Johnston (2017), Avery et al. (2023), and Chen et al. (2023) characterized D_5 + OH SOSiA with mass spectrometry and found spectra indicative of oligomers. The formation of oligomers may reduce the bulk volatility by more than one bin and change the gas-particle equilibrium timescales (Berkemeier et al., 2020). Here, we incorporate $k_{age,gas}$ and a simple "bin-hopping" approach to illustrate that a change in the volatility distribution with OH_{exp} can adequately capture the Y_{SOSiA} variation in the literature. Future work with more sophisticated chemical models should close that gap further.

4 Conclusions and Atmospheric Implications

With a PAM-OFR, PTR-MS, and SMPS, we studied the formation of VOP and SOSiA under various OH_{exp} conditions. Using a simplified VOP oxidation scheme (Eqs. (R5) and (R6)), we find that the VOP of tentatively identified siloxanols and formate esters have shorter OH-oxidation lifetimes than their precursor D_5 (Table S7). In addition, we find the mass yield of HCHO of D_5 comparable to that of isoprene or aromatics (Millet et al., 2006), suggesting that D_5 siloxane is a potential O_3-contributing species in downwind scenarios. We find Y_{HCOOH} ranging from 45 – 127 %, which suggests that D_5 + OH is a source of atmospheric HCOOH, albeit smaller than isoprene which is emitted in higher amounts by orders of magnitude.

An aging-VBS model incorporating OH_{exp} and chemical aging adequately describes gas-particle partitioning at atmospheric OH_{exp} and C_{OA}. Based on these experiments, low-NO_x Y_{SOSiA} should be < 5 % under commonly observed atmospheric OH_{exp} < 5×10^{11} s cm^{-3} (Fig. 6a1). The first-generation products of D_5 + OH are likely volatile, but their volatility decreases with increasing OH_{exp} (Fig. 5). This evolution in volatility suggests that further oxidation of secondary products would reduce the volatility enough to form SOSiA. Unlike α-pinene (Isaacman-VanWertz et al., 2018) or other precursors for SOA, D_5 + OH does not appear to produce low-volatile species within a single oxidation step. Instead, additional OH_{exp} is needed to form aerosol, which suggests that multiple oxidation steps lead to gradual decrease of product volatility. Hence, concepts that can be successfully applied to SOA formation may not accurately capture SOSiA formation, for which models must consider chemical aging. In the atmosphere, SOSiA from D_5 + OH may be easier to detect downwind of urban sources due to the higher OH_{exp} and dilution/removal of competing OH-reactive species.

Based on KinSim calculations (Sect. S5), we expect that the RO_2 fate is dominated by RO_2 + HO_2 and RO_2 + OH, which is consistent with the calculations performed by Avery et al. (2023). However, we note that the reaction rate coefficients of RO_2 and its subsequent products are uncertain for D_5, and we cannot directly address the atmospheric relevance of these calculated RO_2 fates at this time. To improve Y_{SOSiA} parameterizations for the atmosphere, there is a need to study the impact NO_x has on siloxane RO_2 chemistry, given that siloxanes are likely emitted from urban sources where [NO_x] is high. In such scenarios, RO_2 + NO_x is likely an important fate (Peng et al., 2019; Newland et al., 2021). Han et al. (2022) found that the addition of N_2O into their OFR would reduce Y_{SOSiA}, although the cause is unclear. However, Charan et al. (2022) did not find Y_{SOSiA} to change with NO_x in their chamber experiments, which is consistent with rapid RO formation across RO_2 fates. Quantifying secondary species across RO_2 fates and identifying their subsequent oxidation reactions may also be useful to adapt the D_5 oxidation mechanism into more sophisticated chemical kinetics models.

We also find that the aging-VBS model is sensitive to $k_{age,particle}$ (Fig. S11) and not sensitive to $k_{age,gas}$ (Fig. S12), suggesting that heterogeneous aging should be considered in these models. The condensation timescale calculations suggest that the loss of low-volatile species to the wall is small (Sect. S1.3), however, these calculations assume a high mass accommodation

coefficient for SOSiA and do not account for particle nucleation. Should particle nucleation be delayed or happen slowly, the gas wall loss may be higher than expected, leading to under quantification of SOSiA. Furthermore, the aging-VBS model assumes that $k_{age,gas}$ is uniform across products or that chemical aging results in a ten-fold decrease in volatility.

While the proposed model assumes that the particles are internally well mixed, the high [OH] used in OFRs may induce faster radical reactions and dimerization near the particle surface (Zhao et al., 2019), which affects particle composition and equilibrium timescales. While dimers and oligomers have been found in SOSiA (Wu and Johnston, 2017; Avery et al., 2023; Chen et al., 2023), the model currently does not account for particle-phase oligomer formation. How oligomerization in the D_5 + OH SOSiA system evolves the volatility distribution and particle properties is currently not considered in the aging-VBS model. Moreover, high degrees of oxidation should lead to fragmentation and increasing volatility (Isaacman-VanWertz et al., 2018), which is also not considered in the aging-VBS model. Hence, multiphase modeling to evaluate SOSiA chemistry and translate experimental findings to atmospheric conditions remains a direction for future research.

Appendix A Abbreviations

C_{OA}: organic aerosol mass loading
C*: effective saturation mass concentration
D_5: decamethylcyclopentasiloxane
EVR: extended volatility range
ID: inner diameter of tubing
I_{254}, I_{185}: flux of 254 and 185 nm photons
OA: organic aerosol
OD: outer diameter of tubing
OFR: oxidation flow reactor
OH: hydroxyl radical
$[OH]_{avg}$: 24-hour average daily hydroxyl radical concentration
OH_{exp}: hydroxyl radical exposure
OHR_{ext}: external hydroxyl radical reactivity
O_3: ozone
ncps: normalized counts per second
NO_x: nitric oxide and nitrogen dioxide
PAM: potential aerosol mass
PTR: proton transfer reaction
PTR-MS: proton transfer reaction mass spectrometer

RH: relative humidity

RMSE: root mean square error

RO: alkoxyl radical

RO_2: peroxyl radical

SMPS: scanning mobility particle sizer

SOA: secondary organic aerosol

SOSiA: secondary organosiloxane aerosol

UV: ultraviolet radiation

VBS: volatility basis set

VOP: volatile oxidation products

Y_{HCHO}: formaldehyde molar yield from D_5

Y_{HCOOH}: formic acid molar yield from D_5

$Y_{rel,VOP}$: relative molar yield of VOP from D_5

Y_{SOSiA}: SOSiA mass yield from D_5

γ: molar yields extrapolated to when $OH_{exp} \rightarrow 0$

ρ_{SOSiA}: SOSiA aerosol mass density

τ_{res}: residence time

Data Availability

Summary data are available in the supplementary. Additional data will be provided upon reasonable request.

Author ORCID

Hyun Gu Kang: https://orcid.org/0000-0002-3320-9447

Yanfang Chen: https://orcid.org/0000-0002-4415-7398

\Yoojin Park: https://orcid.org/0000-0002-4832-8633

Thomas Berkemeier: https://orcid.org/0000-0001-6390-6465

Hwajin Kim: https://orcid.org/0000-0001-6138-6443

Author Contribution

HGK, YC and YP conducted the experiments. YP performed the offline calibrations of OH exposure on the PAM-OFR. HGK analysed the data. HGK and TB developed the kinetic models. HGK, TB, and HK wrote the manuscript with contributions from all co-authors. HK supervised the experiments, and TB supervised the model analyses.

Competing Interests

TB is a member of the editorial board of Atmospheric Chemistry and Physics, but the peer-review process was guided by an independent editor. The authors declare that they have no other personal nor financial conflicts of interest. Instruments and products used in the research are listed for reference and not as endorsements.

Acknowledgements

This work was supported by the FRIEND Project (Fine Particle Research Initiative in East Asia Considering National Differences), which is funded by the National Research Foundation of Korea (NRF) and the Ministry of Science and ICT of the Republic of Korea (2022M3G1A1020858). This work was also funded by the NRF under NRF-2021R1A2C2004365. HGK is supported by the Max Planck Graduate Center with Johannes Gutenberg University Mainz. APM Engineering (Gyeonggi-do, South Korea) lent the PTR-MS, and the authors thank BO for maintaining it. The authors acknowledge the two anonymous reviewers for their comments, which can be found on the EGUsphere website.

References

Alton, M. W. and Browne, E. C.: Atmospheric Chemistry of Volatile Methyl Siloxanes: Kinetics and Products of Oxidation by OH Radicals and Cl Atoms, Environ Sci Technol, 54, 5992–5999, https://doi.org/10.1021/acs.est.0c01368, 2020.

Alton, M. W. and Browne, E. C.: Atmospheric Degradation of Cyclic Volatile Methyl Siloxanes: Radical Chemistry and Oxidation Products, ACS Environmental Au, https://doi.org/10.1021/acsenvironau.1c00043, 2022.

Arata, C., Misztal, P. K., Tian, Y., Lunderberg, D. M., Kristensen, K., Novoselac, A., Vance, M. E., Farmer, D. K., Nazaroff, W. W., and Goldstein, A. H.: Volatile organic compound emissions during HOMEChem, Indoor Air, 31, 2099–2117, https://doi.org/https://doi.org/10.1111/ina.12906, 2021.

Atkinson, R.: Kinetics of the gas-phase reactions of a series of organosilicon compounds with hydroxyl and nitrate(NO3) radicals and ozone at 297 +- 2 K, Environ Sci Technol, 25, 863–866, https://doi.org/10.1021/es00017a005, 1991.

Atkinson, R., Baulch, D. L., Cox, R. A., Crowley, J. N., Hampson, R. F., Hynes, R. G., Jenkin, M. E., Rossi, M. J., Troe, J., and Subcommittee, I.: Evaluated kinetic and photochemical data for atmospheric chemistry: Volume II – gas phase reactions of organic species, Atmos Chem Phys, 6, 3625–4055, https://doi.org/10.5194/acp-6-3625-2006, 2006.

Avery, A. M., Alton, M. W., Canagaratna, M. R., Krechmer, J. E., Sueper, D. T., Bhattacharyya, N., Hildebrandt Ruiz, L., Brune, W. H., and Lambe, A. T.: Comparison of the Yield and Chemical Composition of Secondary Organic Aerosol Generated from the OH and Cl Oxidation of Decamethylcyclopentasiloxane, ACS Earth Space Chem, https://doi.org/10.1021/acsearthspacechem.2c00304, 2023.

Berkemeier, T., Ammann, M., Krieger, U. K., Peter, T., Spichtinger, P., Pöschl, U., Shiraiwa, M., and Huisman, A. J.: Technical note: Monte Carlo genetic algorithm (MCGA) for model analysis of multiphase chemical kinetics to determine transport and reaction rate coefficients using multiple experimental data sets, Atmos Chem Phys, 17, 8021–8029, https://doi.org/10.5194/acp-17-8021-2017, 2017.

Berkemeier, T., Takeuchi, M., Eris, G., and Ng, N. L.: Kinetic modeling of formation and evaporation of secondary organic aerosol from NO_3 oxidation of pure and mixed monoterpenes, Atmos Chem Phys, 20, 15513–15535, https://doi.org/10.5194/acp-20-15513-2020, 2020.

Berkemeier, T., Mishra, A., Mattei, C., Huisman, A. J., Krieger, U. K., and Pöschl, U.: Ozonolysis of Oleic Acid Aerosol Revisited: Multiphase Chemical Kinetics and Reaction Mechanisms, ACS Earth Space Chem, 5, 3313–3323, https://doi.org/10.1021/acsearthspacechem.1c00232, 2021.

le Breton, M., McGillen, M. R., Muller, J. B. A., Bacak, A., Shallcross, D. E., Xiao, P., Huey, L. G., Tanner, D., Coe, H., and Percival, C. J.: Airborne observations of formic acid using a chemical ionization mass spectrometer, Atmos. Meas. Tech., 5, 3029–3039, https://doi.org/10.5194/amt-5-3029-2012, 2012.

Brown, P., Watts, P., Märk, T. D., and Mayhew, C. A.: Proton transfer reaction mass spectrometry investigations on the effects of reduced electric field and reagent ion internal energy on product ion branching ratios for a series of saturated alcohols, Int J Mass Spectrom, 294, 103–111, https://doi.org/https://doi.org/10.1016/j.ijms.2010.05.028, 2010.

Carter, W. P. L., Pierce, J. A., Malkina, I. L., Luo, D., and Long, W. D.: ENVIRONMENTAL CHAMBER CHAMBER STUDIES STUDIES OF OF MAXIMUM MAXIMUM INCREMENTAL INCREMENTAL REACTIVITIES REACTIVITIES OF OF VOLATILE VOLATILE ORGANIC ORGANIC COMPOUNDS COMPOUNDS, 1993.

Carter, W. P. L., Pierce, J. A., Luo, D., and Malkina, I. L.: Environmental chamber study of maximum incremental reactivities of volatile organic compounds, Atmos Environ, 29, 2499–2511, https://doi.org/https://doi.org/10.1016/1352-2310(95)00149-S, 1995.

Chandramouli, B. and Kamens, R. M.: The photochemical formation and gas–particle partitioning of oxidation products of decamethyl cyclopentasiloxane and decamethyl tetrasiloxane in the atmosphere, Atmos Environ, 35, 87–95, https://doi.org/https://doi.org/10.1016/S1352-2310(00)00289-2, 2001.

Charan, S. M., Huang, Y., Buenconsejo, R. S., Li, Q., Cocker III, D. R., and Seinfeld, J. H.: Secondary organic aerosol formation from the oxidation of decamethylcyclopentasiloxane at atmospherically relevant OH concentrations, Atmos Chem Phys, 22, 917–928, https://doi.org/10.5194/acp-22-917-2022, 2022.

Chen, X., Millet, D. B., Neuman, J. A., Veres, P. R., Ray, E. A., Commane, R., Daube, B. C., McKain, K., Schwarz, J. P., Katich, J. M., Froyd, K. D., Schill, G. P., Kim, M. J., Crounse, J. D., Allen, H. M., Apel, E. C., Hornbrook, R. S., Blake, D R., Nault, B. A., Campuzano-Jost, P., Jimenez, J. L., and Dibb, J. E.: HCOOH in the Remote Atmosphere: Constraints from Atmospheric Tomography (ATom) Airborne Observations, ACS Earth Space Chem, 5, 1436–1454, https://doi.org/10.1021/acsearthspacechem.1c00049, 2021.

Chen, Y., Park, Y., Kang, H. G., Jeong, J., and Kim, H.: Chemical characterization and formation of secondary organosiloxane aerosol (SOSiA) from OH oxidation of decamethylcyclopentasiloxane, Environ. Sci.: Atmos., https://doi.org/10.1039/D2EA00161F, 2023.

Cheng, Z., Qiu, X., Shi, X., and Zhu, T.: Identification of organosiloxanes in ambient fine particulate matters using an untargeted strategy via gas chromatography and time-of-flight mass spectrometry, Environmental Pollution, 271, 116128, https://doi.org/https://doi.org/10.1016/j.envpol.2020.116128, 2021.

Coggon, M. M., McDonald, B. C., Vlasenko, A., Veres, P. R., Bernard, F., Koss, A. R., Yuan, B., Gilman, J. B., Peischl, J., Aikin, K. C., DuRant, J., Warneke, C., Li, S.-M., and de Gouw, J. A.: Diurnal Variability and Emission Pattern of Decamethylcyclopentasiloxane (D5) from the Application of Personal Care Products in Two North American Cities, Environ Sci Technol, 52, 5610–5618, https://doi.org/10.1021/acs.est.8b00506, 2018.

Coggon, M. M., Gkatzelis, G. I., McDonald, B. C., Gilman, J. B., Schwantes, R. H., Abuhassan, N., Aikin, K. C., Arend, M. F., Berkoff, T. A., Brown, S. S., Campos, T. L., Dickerson, R. R., Gronoff, G., Hurley, J. F., Isaacman-VanWertz, G., Koss, A. R., Li, M., McKeen, S. A., Moshary, F., Peischl, J., Pospisilova, V., Ren, X., Wilson, A., Wu, Y., Trainer, M., and Warneke, C. Volatile chemical product emissions enhance ozone and modulate urban chemistry, Proceedings of the National Academy of Sciences, 118, e2026653118, https://doi.org/10.1073/pnas.2026653118, 2021.

Derwent, R. G., Jenkin, M. E., and Saunders, S. M.: Photochemical ozone creation potentials for a large number of reactive hydrocarbons under European conditions, Atmos Environ, 30, 181–199, https://doi.org/https://doi.org/10.1016/1352-2310(95)00303-G, 1996.

Donahue, N. M., Robinson, A. L., Stanier, C. O., and Pandis, S. N.: Coupled partitioning, dilution, and chemical aging of semivolatile organics, Environ Sci Technol, 40, 2635–2643, https://doi.org/10.1021/es052297c, 2006.

Franco, B., Blumenstock, T., Cho, C., Clarisse, L., Clerbaux, C., Coheur, P.-F., de Mazière, M., de Smedt, I., Dorn, H.-P., Emmerichs, T., Fuchs, H., Gkatzelis, G., Griffith, D. W. T., Gromov, S., Hannigan, J. W., Hase, F., Hohaus, T., Jones, N., Kerkweg, A., Kiendler-Scharr, A., Lutsch, E., Mahieu, E., Novelli, A., Ortega, I., Paton-Walsh, C., Pommier, M., Pozzer, A., Reimer, D., Rosanka, S., Sander, R., Schneider, M., Strong, K., Tillmann, R., van Roozendael, M., Vereecken, L., Vigouroux, C., Wahner, A., and Taraborrelli, D.: Ubiquitous atmospheric production of organic acids mediated by cloud droplets, Nature, 593, 233–237, https://doi.org/10.1038/s41586-021-03462-x, 2021.

Friedman, B. and Farmer, D. K.: SOA and gas phase organic acid yields from the sequential photooxidation of seven monoterpenes, Atmos Environ, 187, 335–345, https://doi.org/https://doi.org/10.1016/j.atmosenv.2018.06.003, 2018.

Fu, Z., Xie, H.-B., Elm, J., Guo, X., Fu, Z., and Chen, J.: Formation of Low-Volatile Products and Unexpected High Formaldehyde Yield from the Atmospheric Oxidation of Methylsiloxanes, Environ Sci Technol, 54, 7136–7145, https://doi.org/10.1021/acs.est.0c01090, 2020.

de Gouw, J. and Warneke, C.: Measurements of volatile organic compounds in the earth's atmosphere using proton-transfer-reaction mass spectrometry, Mass Spectrom Rev, 26, 223–257, https://doi.org/https://doi.org/10.1002/mas.20119, 2007.

de Gouw, J., Warneke, C., Karl, T., Eerdekens, G., van der Veen, C., and Fall, R.: Sensitivity and specificity of atmospheric trace gas detection by proton-transfer-reaction mass spectrometry, Int J Mass Spectrom, 223–224, 365–382, https://doi.org/https://doi.org/10.1016/S1387-3806(02)00926-0, 2003.

Graiver, D., Farminer, K. W., and Narayan, R.: A Review of the Fate and Effects of Silicones in the Environment, J Polym Environ, 11, 129–136, https://doi.org/10.1023/A:1026056129717, 2003.

Guenther, a. B., Jiang, X., Heald, C. L., Sakulyanontvittaya, T., Duhl, T., Emmons, L. K., and Wang, X.: The model of emissions of gases and aerosols from nature version 2.1 (MEGAN2.1): An extended and updated framework for modeling biogenic emissions, Geosci Model Dev, 5, 1471–1492, https://doi.org/10.5194/gmd-5-1471-2012, 2012.

Han, C., Yang, H., Li, K., Lee, P., Liggio, J., Leithead, A., and Li, S.-M.: Secondary organic aerosols from OH oxidation of cyclic volatile methyl siloxanes as an important Si source in the atmosphere, Atmos Chem Phys, 22, 10827–10839, https://doi.org/10.5194/acp-22-10827-2022, 2022.

Hazra, M. K., Francisco, J. S., and Sinha, A.: Hydrolysis of Glyoxal in Water-Restricted Environments: Formation of Organic Aerosol Precursors through Formic Acid Catalysis, J Phys Chem A, 118, 4095–4105, https://doi.org/10.1021/jp502126m, 2014.

Horii, Y., Nojiri, K., Minomo, K., Motegi, M., and Kannan, K.: Volatile methylsiloxanes in sewage treatment plants in Saitama, Japan: Mass distribution and emissions, Chemosphere, 233, 677–686, https://doi.org/https://doi.org/10.1016/j.chemosphere.2019.05.247, 2019.

Howard, P. H. and Muir, D. C. G.: Identifying New Persistent and Bioaccumulative Organics Among Chemicals in Commerce, Environ Sci Technol, 44, 2277–2285, https://doi.org/10.1021/es903383a, 2010.

Isaacman-VanWertz, G., Massoli, P., O'Brien, R., Lim, C., Franklin, J. P., Moss, J. A., Hunter, J. F., Nowak, J. B., Canagaratna, M. R., Misztal, P. K., Arata, C., Roscioli, J. R., Herndon, S. T., Onasch, T. B., Lambe, A. T., Jayne, J. T., Su, L., Knopf, D. A., Goldstein, A. H., Worsnop, D. R., and Kroll, J. H.: Chemical evolution of atmospheric organic carbon over multiple generations of oxidation, Nat Chem, 10, 462–468, https://doi.org/10.1038/s41557-018-0002-2, 2018.

Janechek, N. J., Marek, R. F., Bryngelson, N., Singh, A., Bullard, R. L., Brune, W. H., and Stanier, C. O.: Physical properties of secondary photochemical aerosol from OH oxidation of a cyclic siloxane, Atmos Chem Phys, 19, 1649–1664, https://doi.org/10.5194/acp-19-1649-2019, 2019.

Jordan, A., Haidacher, S., Hanel, G., Hartungen, E., Märk, L., Seehauser, H., Schottkowsky, R., Sulzer, P., and Märk, T. D.: A high resolution and high sensitivity proton-transfer-reaction time-of-flight mass spectrometer (PTR-TOF-MS), Int J Mass Spectrom, 286, 122–128, https://doi.org/https://doi.org/10.1016/j.ijms.2009.07.005, 2009.

Kaikiti, C., Stylianou, M., and Agapiou, A.: TD-GC/MS analysis of indoor air pollutants (VOCs, PM) in hair salons, Chemosphere, 294, 133691, https://doi.org/https://doi.org/10.1016/j.chemosphere.2022.133691, 2022.

Kang, E., Root, M. J., Toohey, D. W., and Brune, W. H.: Introducing the concept of Potential Aerosol Mass (PAM), Atmos Chem Phys, 7, 5727–5744, https://doi.org/10.5194/acp-7-5727-2007, 2007.

Katz, E. F., Lunderberg, D. M., Brown, W. L., Day, D. A., Jimenez, J. L., Nazaroff, W. W., Goldstein, A. H., and DeCarlo, P. F.: Large Emissions of Low-Volatility Siloxanes during Residential Oven Use, Environ Sci Technol Lett, 8, 519–524, https://doi.org/10.1021/acs.estlett.1c00433, 2021.

Kessler, S. H., Nah, T., Daumit, K. E., Smith, J. D., Leone, S. R., Kolb, C. E., Worsnop, D. R., Wilson, K. R., and Kroll, J. H. OH-Initiated Heterogeneous Aging of Highly Oxidized Organic Aerosol, J Phys Chem A, 116, 6358–6365, https://doi.org/10.1021/jp212131m, 2012.

Kim, J. and Xu, S.: Quantitative structure-reactivity relationships of hydroxyl radical rate constants for linear and cyclic volatile methylsiloxanes, Environ Toxicol Chem, 36, 3240–3245, https://doi.org/https://doi.org/10.1002/etc.3914, 2017.

Kroll, J. H., Lim, C. Y., Kessler, S. H., and Wilson, K. R.: Heterogeneous Oxidation of Atmospheric Organic Aerosol: Kinetics of Changes to the Amount and Oxidation State of Particle-Phase Organic Carbon, J Phys Chem A, 119, 10767–10783, https://doi.org/10.1021/acs.jpca.5b06946, 2015.

Lee, S., Moon, H.-B., Song, G.-J., Ra, K., Lee, W.-C., and Kannan, K.: A nationwide survey and emission estimates of cyclic and linear siloxanes through sludge from wastewater treatment plants in Korea, Science of The Total Environment, 497–498, 106–112, https://doi.org/https://doi.org/10.1016/j.scitotenv.2014.07.083, 2014.

Lei, Y. D., Wania, F., and Mathers, D.: Temperature-Dependent Vapor Pressure of Selected Cyclic and Linear Polydimethylsiloxane Oligomers, J Chem Eng Data, 55, 5868–5873, https://doi.org/10.1021/je100835n, 2010.

Link, M. F., Nguyen, T. B., Bates, K., Müller, J.-F., and Farmer, D. K.: Can Isoprene Oxidation Explain High Concentrations of Atmospheric Formic and Acetic Acid over Forests?, ACS Earth Space Chem, 4, 730–740, https://doi.org/10.1021/acsearthspacechem.0c00010, 2020.

Lu, D., Tan, J., Yang, X., Sun, X., Liu, Q., and Jiang, G.: Unraveling the role of silicon in atmospheric aerosol secondary formation: a new conservative tracer for aerosol chemistry, Atmos Chem Phys, 19, 2861–2870, https://doi.org/10.5194/acp-19-2861-2019, 2019.

Mao, J., Ren, X., Brune, W. H., Olson, J. R., Crawford, J. H., Fried, A., Huey, L. G., Cohen, R. C., Heikes, B., Singh, H. B., Blake, D. R., Sachse, G. W., Diskin, G. S., Hall, S. R., and Shetter, R. E.: Airborne measurement of OH reactivity during INTEX-B, Atmos Chem Phys, 9, 163–173, https://doi.org/10.5194/acp-9-163-2009, 2009.

Meng, T., Su, S., Cheng, J., Zhong, F., and Tang, Z.: Methylsiloxanes in street dust from Hefei, China: Distribution, sources, and human exposure, Environ Res, 201, 111513, https://doi.org/https://doi.org/10.1016/j.envres.2021.111513, 2021.

Milani, A., Al-Naiema, I. M., and Stone, E. A.: Detection of a secondary organic aerosol tracer derived from personal care products, Atmos Environ, 246, 118078, https://doi.org/https://doi.org/10.1016/j.atmosenv.2020.118078, 2021.

Millet, D. B., Jacob, D. J., Turquety, S., Hudman, R. C., Wu, S., Fried, A., Walega, J., Heikes, B. G., Blake, D. R., Singh, H. B., Anderson, B. E., and Clarke, A. D.: Formaldehyde distribution over North America: Implications for satellite retrievals of formaldehyde columns and isoprene emission, Journal of Geophysical Research: Atmospheres, 111 https://doi.org/https://doi.org/10.1029/2005JD006853, 2006.

Millet, D. B., Baasandorj, M., Farmer, D. K., Thornton, J. A., Baumann, K., Brophy, P., Chaliyakunnel, S., de Gouw, J. A., Graus, M., Hu, L., Koss, A., Lee, B. H., Lopez-Hilfiker, F. D., Neuman, J. A., Paulot, F., Peischl, J., Pollack, I. B., Ryerson, T. B., Warneke, C., Williams, B. J., and Xu, J.: A large and ubiquitous source of atmospheric formic acid, Atmos Chem Phys, 15, 6283–6304, https://doi.org/10.5194/acp-15-6283-2015, 2015.

Müller, M., Mikoviny, T., and Wisthaler, A.: Detector aging induced mass discrimination and non-linearity effects in PTR-ToF-MS, Int J Mass Spectrom, 365–366, 93–97, https://doi.org/https://doi.org/10.1016/j.ijms.2013.12.008, 2014.

Newland, M. J., Bryant, D. J., Dunmore, R. E., Bannan, T. J., Acton, W. J. F., Langford, B., Hopkins, J. R., Squires, F. A., Dixon, W., Drysdale, W. S., Ivatt, P. D., Evans, M. J., Edwards, P. M., Whalley, L. K., Heard, D. E., Slater, E. J., Woodward-Massey, R., Ye, C., Mehra, A., Worrall, S. D., Bacak, A., Coe, H., Percival, C. J., Hewitt, C. N., Lee, J. D., Cui, T., Surratt, J. D., Wang, X., Lewis, A. C., Rickard, A. R., and Hamilton, J. F.: Low-NO atmospheric oxidation pathways in a polluted megacity, Atmos Chem Phys, 21, 1613–1625, https://doi.org/10.5194/acp-21-1613-2021, 2021.

Odum, J. R., Hoffmann, T., Bowman, F., Collins, D., Flagan, R. C., and Seinfeld, J. H.: Gas/Particle Partitioning and Secondary Organic Aerosol Yields, Environ Sci Technol, 30, 2580–2585, https://doi.org/10.1021/es950943+, 1996.

Palm, B. B., Campuzano-Jost, P., Ortega, A. M., Day, D. A., Kaser, L., Jud, W., Karl, T., Hansel, A., Hunter, J. F., Cross, E S., Kroll, J. H., Peng, Z., Brune, W. H., and Jimenez, J. L.: In situ secondary organic aerosol formation from ambient pine forest air using an oxidation flow reactor, Atmos Chem Phys, 16, 2943–2970, https://doi.org/10.5194/acp-16-2943-2016, 2016.

Peng, Z. and Jimenez, J. L.: Radical chemistry in oxidation flow reactors for atmospheric chemistry research, Chem. Soc. Rev., 49, 2570–2616, https://doi.org/10.1039/C9CS00766K, 2020.

Peng, Z., Lee-Taylor, J., Orlando, J. J., Tyndall, G. S., and Jimenez, J. L.: Organic peroxy radical chemistry in oxidation flow reactors and environmental chambers and their atmospheric relevance, Atmos Chem Phys, 19, 813–834, https://doi.org/10.5194/acp-19-813-2019, 2019.

Pennington, E. A., Seltzer, K. M., Murphy, B. N., Qin, M., Seinfeld, J. H., and Pye, H. O. T.: Modeling secondary organic aerosol formation from volatile chemical products, Atmos Chem Phys, 21, 18247–18261, https://doi.org/10.5194/acp-21-18247-2021, 2021.

Piel, F., Müller, M., Winkler, K., af Sätra, J., and Wisthaler, A.: Introducing the extended volatility range proton-transfer-reaction mass spectrometer (EVR PTR-MS), Atmos Meas Tech, 14, 1355–1363, https://doi.org/10.5194/amt-14-1355-2021, 2021.

Robinson, A. L., Donahue, N. M., Shrivastava, M. K., Weitkamp, E. A., Sage, A. M., Grieshop, A. P., Lane, T. E., Pierce, J R., and Pandis, S. N.: Rethinking Organic Aerosols: Semivolatile Emissions and Photochemical Aging, Science (1979), 315, 1259–1262, https://doi.org/10.1126/science.1133061, 2007.

Rücker, C. and Kümmerer, K.: Environmental Chemistry of Organosiloxanes, Chem Rev, 115, 466–524, https://doi.org/10.1021/cr500319v, 2015.

Safron, A., Strandell, M., Kierkegaard, A., and Macleod, M.: Rate Constants and Activation Energies for Gas-Phase Reactions of Three Cyclic Volatile Methyl Siloxanes with the Hydroxyl Radical, Int J Chem Kinet, 47, 420–428, https://doi.org/https://doi.org/10.1002/kin.20919, 2015.

Schweigkofler, M. and Niessner, R.: Determination of Siloxanes and VOC in Landfill Gas and Sewage Gas by Canister Sampling and GC-MS/AES Analysis, Environ Sci Technol, 33, 3680–3685, https://doi.org/10.1021/es9902569, 1999.

Seltzer, K. M., Pennington, E., Rao, V., Murphy, B. N., Strum, M., Isaacs, K. K., and Pye, H. O. T.: Reactive organic carbon emissions from volatile chemical products, Atmos Chem Phys, 21, 5079–5100, https://doi.org/10.5194/acp-21-5079-2021, 2021a.

Seltzer, K. M., Murphy, B. N., Pennington, E. A., Allen, C., Talgo, K., and Pye, H. O. T.: Volatile Chemical Product Enhancements to Criteria Pollutants in the United States, Environ Sci Technol, https://doi.org/10.1021/acs.est.1c04298, 2021b.

Sommerlade, R., Parlar, H., Wrobel, D., and Kochs, P.: Product analysis and kinetics of the gas-phase reactions of selected organosilicon compounds with OH radicals using a smog chamber-mass spectrometer system, Environ Sci Technol, 27, 2435–2440, https://doi.org/10.1021/es00048a019, 1993.

Sommers, J. M., Stroud, C. A., Adam, M. G., O'Brien, J., Brook, J. R., Hayden, K., Lee, A. K. Y., Li, K., Liggio, J., Mihele, C., Mittermeier, R. L., Stevens, R. G., Wolde, M., Zuend, A., and Hayes, P. L.: Evaluating SOA formation from different sources of semi- and intermediate-volatility organic compounds from the Athabasca oil sands, Environmental Science: Atmospheres, 2, 469–490, https://doi.org/10.1039/D1EA00053E, 2022.

Song, K., Gong, Y., Guo, S., Lv, D., Wang, H., Wan, Z., Yu, Y., Tang, R., Li, T., Tan, R., Zhu, W., Shen, R., and Lu, S.: Investigation of partition coefficients and fingerprints of atmospheric gas- and particle-phase intermediate volatility and semi-volatile organic compounds using pixel-based approaches, J Chromatogr A, 1665, 462808, https://doi.org/https://doi.org/10.1016/j.chroma.2022.462808, 2022.

Spivack, J. L., Pohl, E. R., and Kochs, P.: Organoalkoxysilanes, Organosilanols, and Organosiloxanols, in: Organosilicon Materials, edited by: Chandra, G., Springer Berlin Heidelberg, Berlin, Heidelberg, 105–135, https://doi.org/10.1007/978-3-540-68331-5_5, 1997.

Stevens, C.: Environmental degradation pathways for the breakdown of polydimethylsiloxanes, J Inorg Biochem, 69, 203–207, https://doi.org/https://doi.org/10.1016/S0162-0134(97)10019-8, 1998.

Tang, X., Misztal, P. K., Nazaroff, W. W., and Goldstein, A. H.: Siloxanes Are the Most Abundant Volatile Organic Compound Emitted from Engineering Students in a Classroom, Environ Sci Technol Lett, 2, 303–307, https://doi.org/10.1021/acs.estlett.5b00256, 2015.

Tansel, B. and Surita, S. C.: Historical and projected trends of siloxane use in consumer products, associated impacts on municipal solid waste and landfill gas utilization, International Journal of Environmental Science and Technology, 14, 795–802, https://doi.org/10.1007/s13762-016-1186-x, 2017.

Tran, T. M. and Kannan, K.: Occurrence of cyclic and linear siloxanes in indoor air from Albany, New York, USA, and its implications for inhalation exposure, Science of The Total Environment, 511, 138–144, https://doi.org/https://doi.org/10.1016/j.scitotenv.2014.12.022, 2015.

TSI Inc.: MEASURING NANOPARTICLE SIZE DISTRIBUTIONS IN REAL-TIME: KEY FACTORS FOR ACCURACY, 2012.

Wang, N., Ernle, L., Bekö, G., Wargocki, P., and Williams, J.: Emission Rates of Volatile Organic Compounds from Humans, Environ Sci Technol, 56, 4838–4848, https://doi.org/10.1021/acs.est.1c08764, 2022.

Whelan, M. J. and Kim, J.: Application of multimedia models for understanding the environmental behavior of volatile methylsiloxanes: Fate, transport, and bioaccumulation, Integr Environ Assess Manag, n/a, 1–23, https://doi.org/https://doi.org/10.1002/ieam.4507, 2021.

Whelan, M. J., Estrada, E., and van Egmond, R.: A modelling assessment of the atmospheric fate of volatile methyl siloxanes and their reaction products, Chemosphere, 57, 1427–1437, https://doi.org/https://doi.org/10.1016/j.chemosphere.2004.08.100 2004.

Wu, Y. and Johnston, M. V: Aerosol Formation from OH Oxidation of the Volatile Cyclic Methyl Siloxane (cVMS) Decamethylcyclopentasiloxane, Environ Sci Technol, 51, 4445–4451, https://doi.org/10.1021/acs.est.7b00655, 2017.

Xiang, X., Liu, N., Xu, L., and Cai, Y.: Review of recent findings on occurrence and fates of siloxanes in environmental compartments, Ecotoxicol Environ Saf, 224, 112631, https://doi.org/https://doi.org/10.1016/j.ecoenv.2021.112631, 2021.

Xiao, R., Zammit, I., Wei, Z., Hu, W.-P., MacLeod, M., and Spinney, R.: Kinetics and Mechanism of the Oxidation of Cyclic Methylsiloxanes by Hydroxyl Radical in the Gas Phase: An Experimental and Theoretical Study, Environ Sci Technol, 49, 13322–13330, https://doi.org/10.1021/acs.est.5b03744, 2015.

Xu, J., Harrison, R. M., Song, C., Hou, S., Wei, L., Fu, P., Li, H., Li, W., and Shi, Z.: PM2.5-bound silicon-containing secondary organic aerosols (Si-SOA) in Beijing ambient air, Chemosphere, 288, 132377, https://doi.org/https://doi.org/10.1016/j.chemosphere.2021.132377, 2022.

Xu, N. and Collins, D. R.: Design and characterization of a new oxidation flow reactor for laboratory and long-term ambient studies, Atmos Meas Tech, 14, 2891–2906, https://doi.org/10.5194/amt-14-2891-2021, 2021.

Yu, S.: Role of organic acids (formic, acetic, pyruvic and oxalic) in the formation of cloud condensation nuclei (CCN): a review, Atmos Res, 53, 185–217, https://doi.org/https://doi.org/10.1016/S0169-8095(00)00037-5, 2000.

Yuan, B., Veres, P. R., Warneke, C., Roberts, J. M., Gilman, J. B., Koss, A., Edwards, P. M., Graus, M., Kuster, W. C., Li, S.-M., Wild, R. J., Brown, S. S., Dubé, W. P., Lerner, B. M., Williams, E. J., Johnson, J. E., Quinn, P. K., Bates, T. S., Lefer, B., Hayes, P. L., Jimenez, J. L., Weber, R. J., Zamora, R., Ervens, B., Millet, D. B., Rappenglück, B., and de Gouw, J. A.: Investigation of secondary formation of formic acid: urban environment vs. oil and gas producing region, Atmos. Chem. Phys., 15, 1975–1993, https://doi.org/10.5194/acp-15-1975-2015, 2015.

Zhao, B., Wang, S., Donahue, N. M., Chuang, W., Hildebrandt Ruiz, L., Ng, N. L., Wang, Y., and Hao, J.: Evaluation of One-Dimensional and Two-Dimensional Volatility Basis Sets in Simulating the Aging of Secondary Organic Aerosol with Smog-Chamber Experiments, Environ Sci Technol, 49, 2245–2254, https://doi.org/10.1021/es5048914, 2015.

Zhao, Z., Tolentino, R., Lee, J., Vuong, A., Yang, X., and Zhang, H.: Interfacial Dimerization by Organic Radical Reactions during Heterogeneous Oxidative Aging of Oxygenated Organic Aerosols, J Phys Chem A, 123, 10782–10792, https://doi.org/10.1021/acs.jpca.9b10779, 2019.

Table 1. Summary of SOSiA mass yields (Y_{SOSiA}) with aerosol sampling line corrections assuming ρ_{SOSiA} = 1.07 g cm^{-3} for all experiments. [H_2O] is the molar mixing ratio of H_2O in air. For C_{OA} and [D_5], the errors are the standard deviation of the data points averaged, while for Y_{SOSiA}, they are calculated with error propagation. For reference, at 25 °C and 1 atm, 1 ppb of D_5 is ~15 µg m^{-3} and one day equivalent of OH_{exp} is ~1.3 × 10^{11} s cm^{-3} at a daily $[OH]_{avg}$ of 1.5 × 10^6 cm^{-3}.

Experiment	Y_{SOSiA} (%)	[H_2O] (%)	C_{OA} (µg m^{-3})	OH_{exp} (s cm^{-3})	[OH] (cm^{-3})	$[D_5]_0$ (ppb)	$1 - [D_5]_{final}/[D_5]_0$
1	5.9 ± 0.9	0.892	10.5 ± 0.7	1.73 × 10^{11}	9.59 × 10^8	43.4 ± 1.3	0.292
2	4.9 ± 0.6	0.828	19.0 ± 0.6	1.90 × 10^{11}	1.06 × 10^9	85.7 ± 2.5	0.316
3	3.3 ± 0.6	0.742	17.7 ± 0.5	1.26 × 10^{11}	6.99 × 10^8	165.8 ± 4.5	0.222
4	19.5 ± 1.5	1.95	75.2 ± 1.9	4.66 × 10^{11}	2.59 × 10^9	44.0 ± 1.7	0.606
5	29.3 ± 2.7	2.06	179.2 ± 3.1	3.80 × 10^{11}	2.11 × 10^9	78.3 ± 3.2	0.532
6	26.5 ± 1.8	2.09	286.2 ± 7.1	3.12 × 10^{11}	1.73 × 10^9	157.8 ± 3.6	0.464
7	8.6 ± 0.5	0.733	36.8 ± 1.3	5.76 × 10^{11}	3.20 × 10^9	43.8 ± 1.3	0.684
8	18.6 ± 1.7	0.736	118.6 ± 5.6	4.00 × 10^{11}	2.22 × 10^9	78.9 ± 3.2	0.550
9	21.8 ± 1.1	0.797	304.5 ± 2.8	4.19 × 10^{11}	2.33 × 10^9	166.8 ± 4.1	0.567
10	39.8 ± 2.2	1.93	212.9 ± 8.1	9.01 × 10^{11}	5.00 × 10^9	43.8 ± 1.4	0.835
11	47.4 ± 1.9	2.08	420.2 ± 3.0	7.78 × 10^{11}	4.32 × 10^9	76.5 ± 2.2	0.789
12	54.0 ± 2.4	2.15	965.7 ± 25	7.39 × 10^{11}	4.10 × 10^9	156.9 ± 3.9	0.772
13	4.7 ± 1.7	0.712	3.9 ± 0.3	8.70 × 10^{10}	7.25 × 10^8	37.9 ± 1.6	0.160
14	1.9 ± 0.4	0.718	4.1 ± 0.3	1.09 × 10^{11}	9.10 × 10^8	80.8 ± 2.3	0.196
15	1.1 ± 0.3	0.704	3.7 ± 0.7	8.29 × 10^{10}	6.91 × 10^8	162.8 ± 4.9	0.153

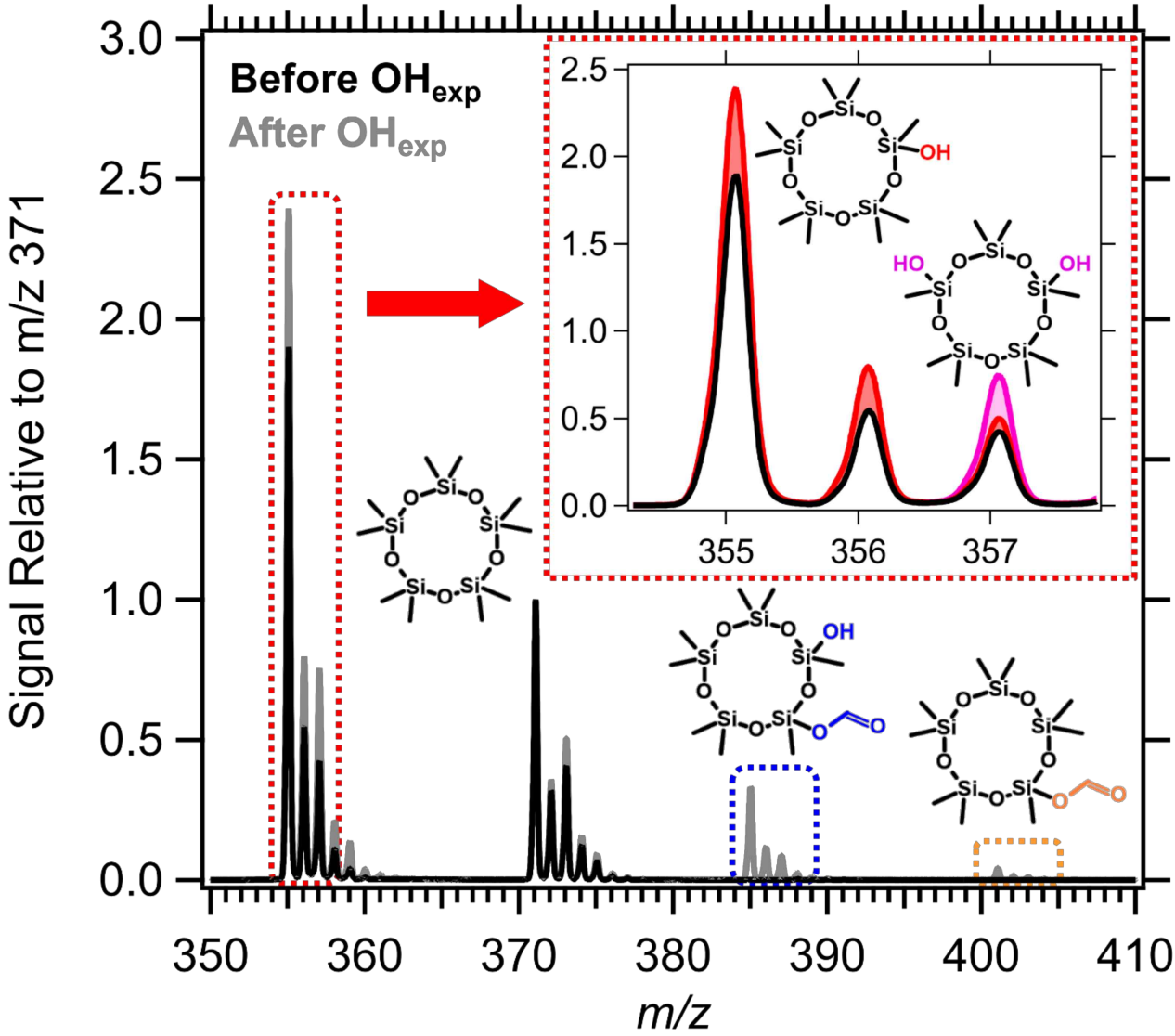

Figure 1. Example PTR-MS mass spectra from experiment 12 and proposed VOP ions. For visualization, the signal intensities, before (black) and after (grey) oxidation, are shown relative to the maximum signal intensity of the $[D_5]H^+$ ion at *m/z* 371, which is set to 1. The multifunctional species (blue, pink) are expected to be formed through multiple steps of OH-oxidation. The red and pink areas in the inset each refer to the enhancement in signal attributed to $D_4T(OH)$ and $D_3T_2(OH)_2$ over that of the $-CH_4$ fragment of $[D_5]H^+$ and isotope signals, respectively.

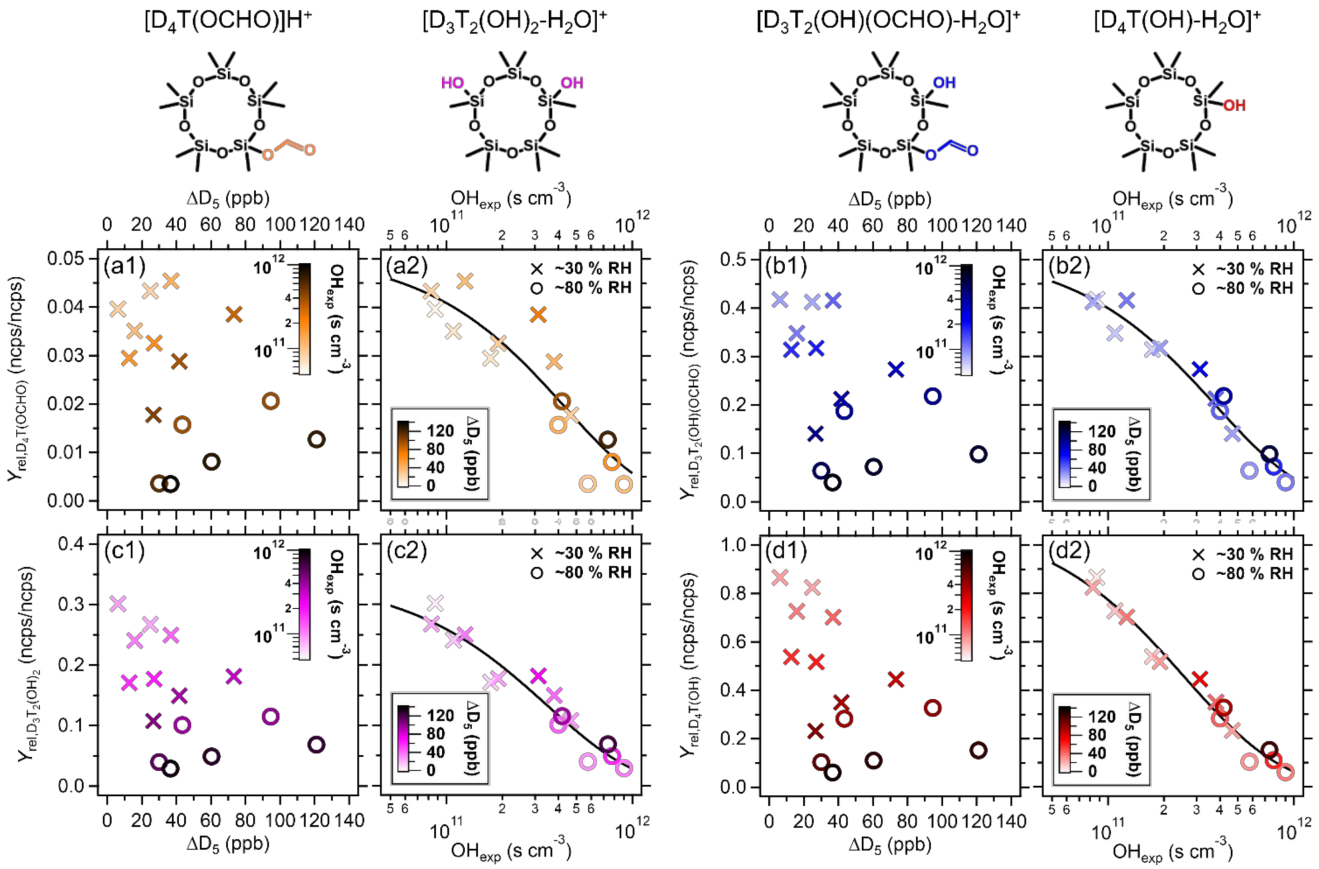

Figure 2. Relative molar yields of VOP as a function of OH_{exp} and D_5 consumed. (a1, a2) $D_4T(OCHO)$, (b1, b2) $D_3T_2(OH)(OCHO)$, (c1, c2) $D_3T_2(OH)_2$, and (d1, d2) $D_4T(OH)$. The colors correspond to the attributed mass ions and molecular structures shown at the top. We did not have a calibration for the suspected VOP, so the y-axes are relative molar yields (ncps/ncps) calculated with the change in signal attributed to each VOP and that of D_5 at *m/z* 371. The relative molar yields decrease with OH_{exp}, which is used to fit their OH-oxidation rate coefficients and γ_i (black lines).

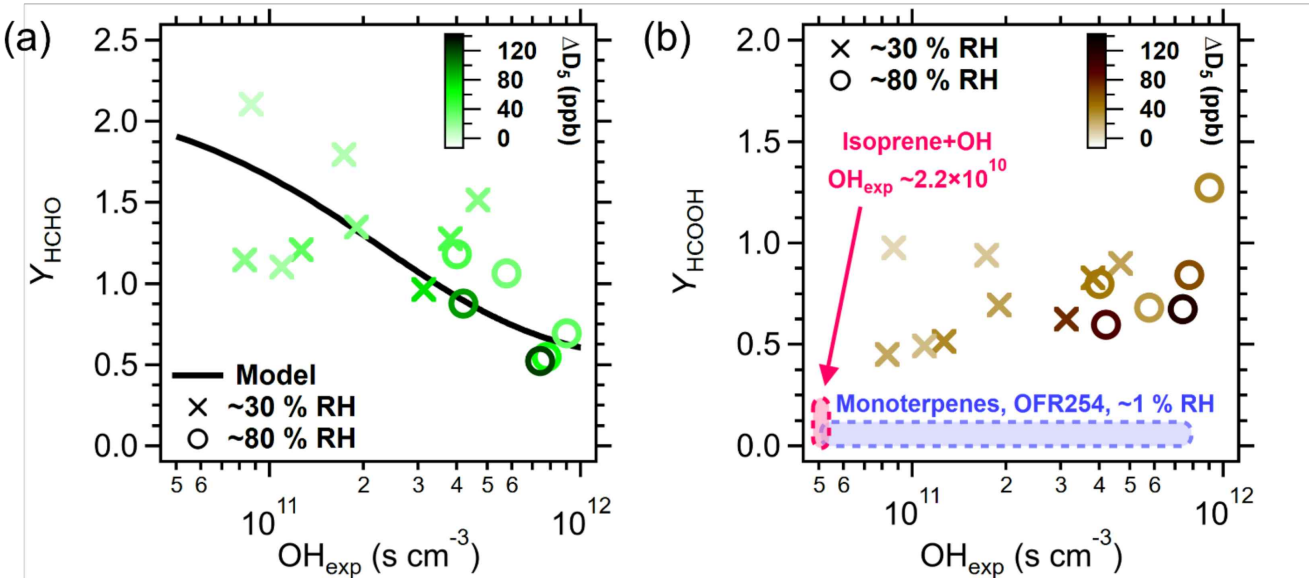

Figure 3. Experimental molar yields of selected VOP: (a) HCHO and (b) HCOOH as functions of OH_{exp}. The blue shaded area in (b) is the range of Y_{HCOOH} (< 10 %) measured by Friedman and Farmer (2018) with monoterpenes under low RH and low NO_x conditions. The pink shaded area refers to Y_{HCOOH} from isoprene + OH chamber experiments (Link et al., 2020) at lower OH_{exp}.

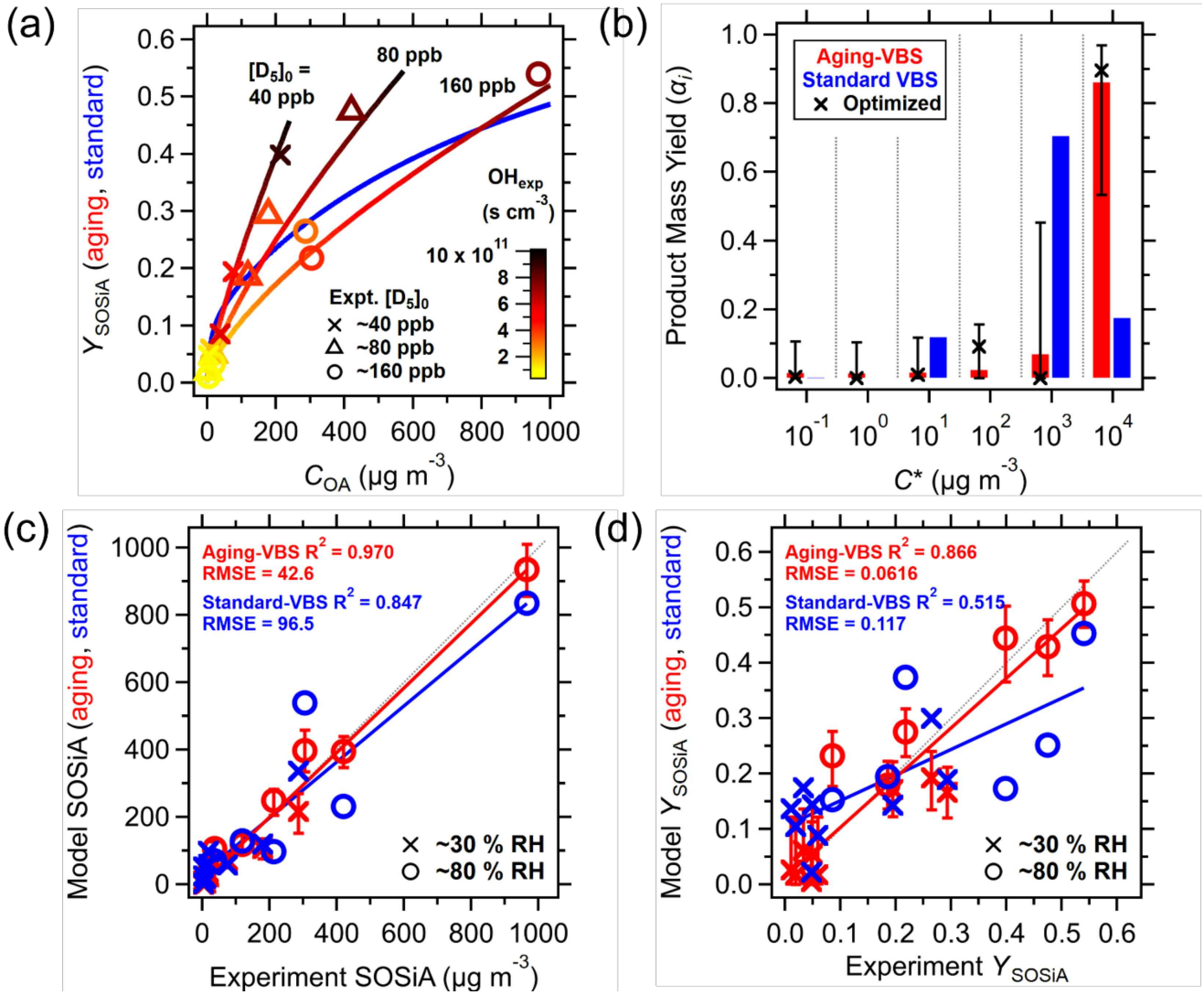

Figure 4. Application of standard-VBS and aging-VBS models to experimental data. (a) Y_{SOSiA} as a function of C_{OA}, where the Y_{SOSiA} appears to be correlated with OH_{exp}. The standard-VBS model is shown in blue, and the aging-VBS model is shown with OH_{exp} (color scale) as it is a kinetic model. (b) VBS product mass yields for each volatility bin. For the aging-VBS, the values are those of the first-generation products. (c) Comparison of SOSiA mass concentrations and (d) comparison of Y_{SOSiA} between the aging-VBS and standard-VBS models against measurements. The error bars indicate the minimum and maximum values from the parameter fit ensemble. The aging-VBS model shows a lower RMSE and higher R^2."

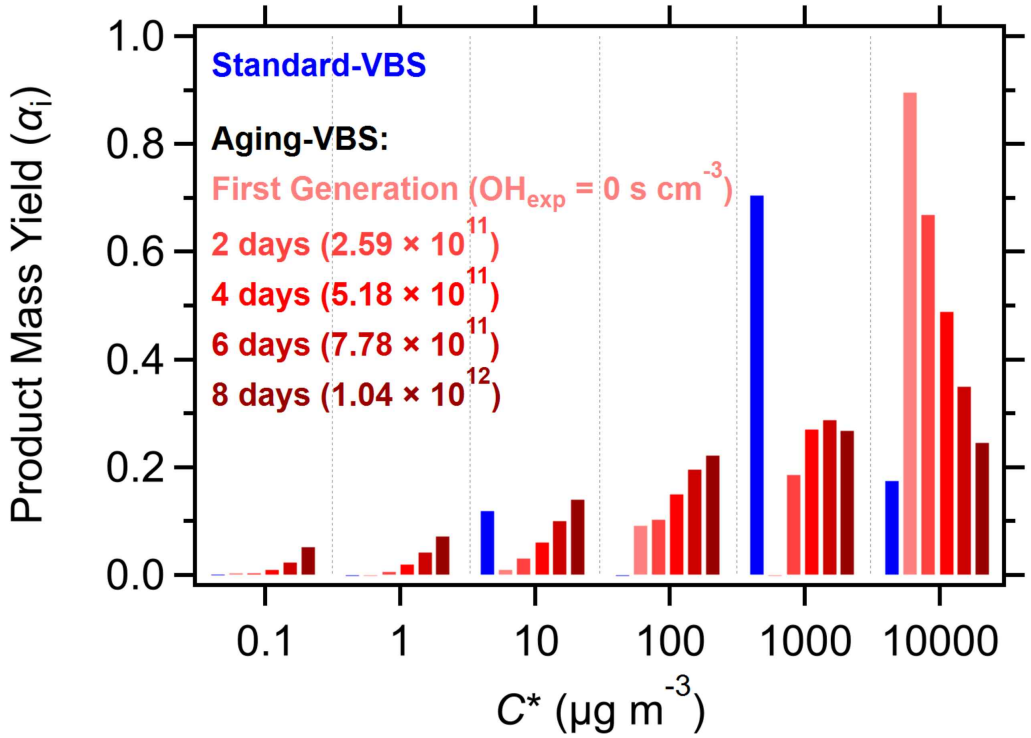

Figure 5. Evolution of the volatility distribution with OH_{exp}. The standard-VBS model parameterization (blue bars) is dominated by the C* = 1 000 µg m^{-3} volatility bin. In the aging-VBS model, the first-generation volatility distribution is dominated by the highest volatility bin (C* = 10 000 µg m^{-3}) but decreases with increasing OH_{exp} (red bars).

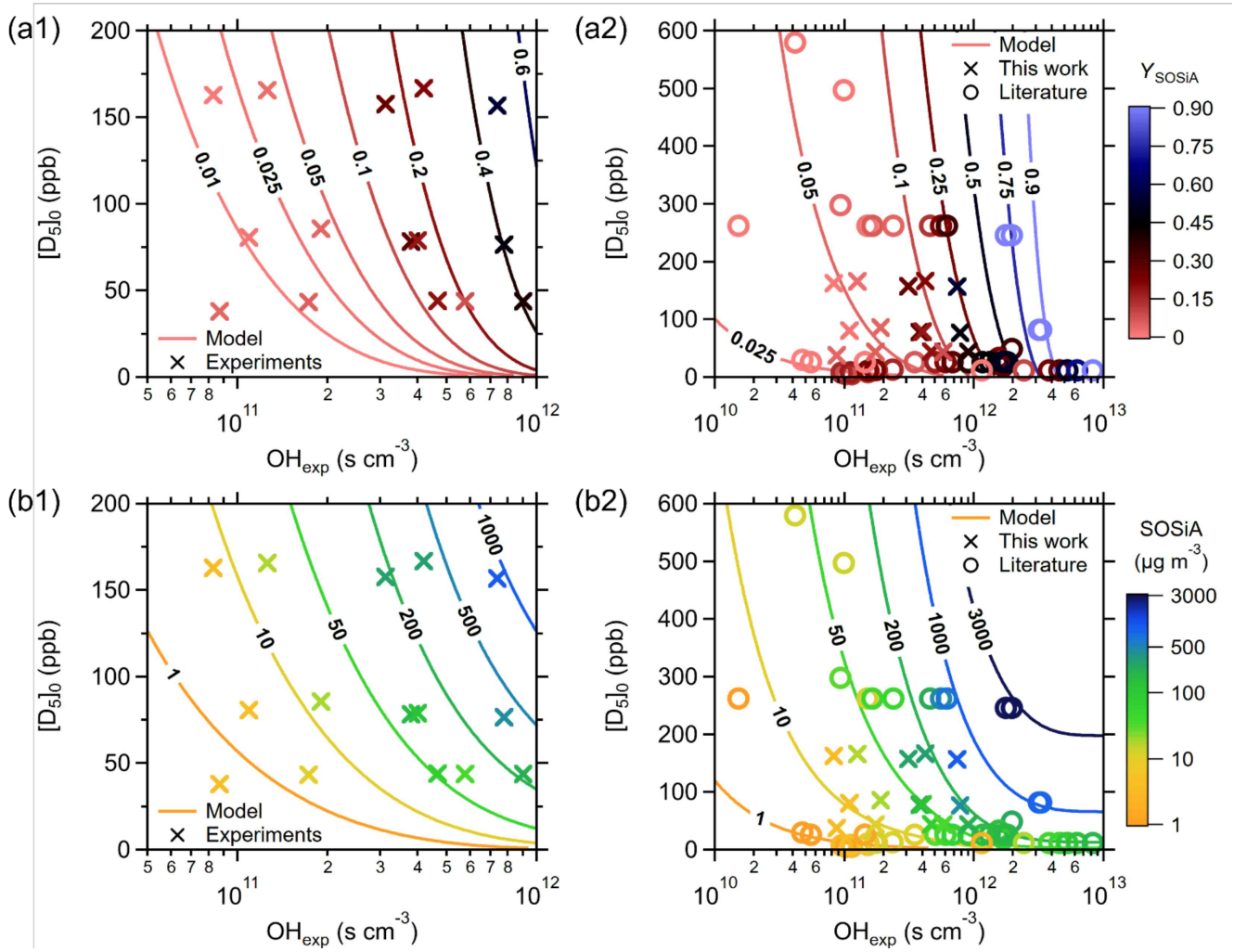

Figure 6. Comparison of experiments, model results, and literature values. (a) Y_{SOSiA} and (b) SOSiA mass concentrations as a function of $[D_5]_0$ and OH_{exp}. The aging VBS-model is fit using experimental data from (1) this study and (2) including those in the literature. SOSiA formation generally increases with $[D_5]_0$ and OH_{exp}. The aging-VBS can capture the broad range of Y_{SOSiA} reported in the literature.